Comparing Secondary Organic Aerosols Schemes Implemented in Current Chemical Transport Models and the Policy Implications of Uncertainties

Ling Huang[1], Benjie Chen[1], Zi'ang Wu[1], Katie Tuite[2], Pradeepa Vennam[2], Greg Yarwood[2,*], Li Li[1,*]

[1]School of Environmental and Chemical Engineering, Shanghai University, Shanghai, 200444, China

[2]Ramboll, Novato, California, 94945, USA

Correspondence to: Greg Yarwood (gyarwood@ramboll.com), Li Li (lily@shu.edu.cn)

Abstract

Secondary organic aerosol (SOA) constitutes a major component of fine particulate matter ($PM_{2.5}$) that models must account for to assess how human activities influence air quality, climate, and public health. We characterize the current state of SOA modeling by analyzing eight SOA schemes implemented in five widely used air quality models: CAMx, CMAQ, GEOS-Chem, WRF-Chem and CHIMERE. We performed offline calculations to compare non-aged SOA yields, the effects of SOA aging processes, and the influence of NOx conditions on yields. Our objective is to understand variation rather than to identify a superior scheme. We find significant discrepancies in SOA yields with the ratio of maximum to minimum non-aged yield spans from 1.8 to over 1000, depending upon precursor. The impact of nitrogen oxide (NOx) conditions on SOA yields is also highly variable among schemes. While some schemes include SOA aging, their treatments differ substantially, with some schemes showing large increases in SOA mass, while others exhibit minimal changes. Box model simulations confirmed the substantial discrepancies in predicted SOA concentrations and their responses to precursor emission changes. The substantial differences among current SOA schemes highlight a lack of consensus within the air quality modelling community. Evaluating model simulation results using ambient measurements is unlikely to resolve these discrepancies because uncertainties in SOA formation and precursor emissions are deeply intertwined. The limitations of current SOA schemes should be recognized and acknowledged because model choice can

greatly influence predicted SOA concentrations and their evolution, ultimately impacting air quality forecasts, assessments, and regulatory decisions.

Keywords: Secondary organic aerosol (SOA), chemical transport model (CTM), two-product, volatility basis set (VBS), SOA yields, CAMx, CMAQ, GEOS-Chem, WRF-Chem, CHIMERE

1. Introduction

Organic Aerosol (OA) contributes a large fraction of fine particulate matter ($PM_{2.5}$) due to primary OA emissions (POA) and the formation of secondary OA (SOA) from anthropogenic, biogenic, and biomass burning sources (Donahue et al., 2006; Huang et al., 2014; Tsimpidi et al., 2016). SOA precursor emissions include traditional volatile organic compounds (VOC) as well as non-traditional intermediate and semi-volatile VOC (IVOC and SVOC, respectively) whereas POA are directly emitted from combustion sources. Recent studies report that volatile chemical products (VCPs) are increasingly important contributors to SOA formation (Pennington et al., 2021; Sasidharan et al., 2023). Chemical transport models (CTMs) are essential tools for understanding the sources and transport of OA as well as assessing the effectiveness of mitigation strategies (e.g. Pye et al., 2021; Chang et al., 2022; Chen et al., 2024; Pennington et al., 2024; Vitali et al., 2024). However, accurately modeling SOA formation in CTMs has posed persistent challenges due to the intricate nature of SOA formation processes (Li et al., 2023). Scientific understanding of SOA formation pathways is continuously evolving. Therefore, it is crucial to review the state of science on SOA formation implemented in different CTMs and identify existing knowledge gaps.

In general, CTMs adopt one of two approaches for SOA simulation: the two-product scheme (Figure 1) or the volatility basis set (VBS) scheme (Figure 2a). Two-product schemes apply the absorptive gas-particle partitioning theory of Pankow (1994) using only two surrogate products to represent all of the condensable gases (CGs) formed when SOA precursors are oxidized in the gas phase by OH radical, ozone (O_3), or NO_3 radical, e.g.:

$$\text{SOA precursor} + \text{OH} \rightarrow \alpha_1 \times \text{CG1} + \alpha_2 \times \text{CG2} \quad \text{R1}$$

where CG1 and CG2 have different saturation concentration (C*); α_1 and α_2 are molar stoichiometric yields. The α and C* values for CG1 and CG2 are fitted to SOA formation observed in chamber experiments. SOA formation depends on the total amount of OA present (Pankow, 1994) and consequently SOA formation depends on POA. POA is usually treated as non-volatile in two-product schemes (e.g., Strader et al., 1999; Schell et al., 2001) but can be treated as semi-volatile in a modified two-product scheme (e.g. Huang et al. 2024).

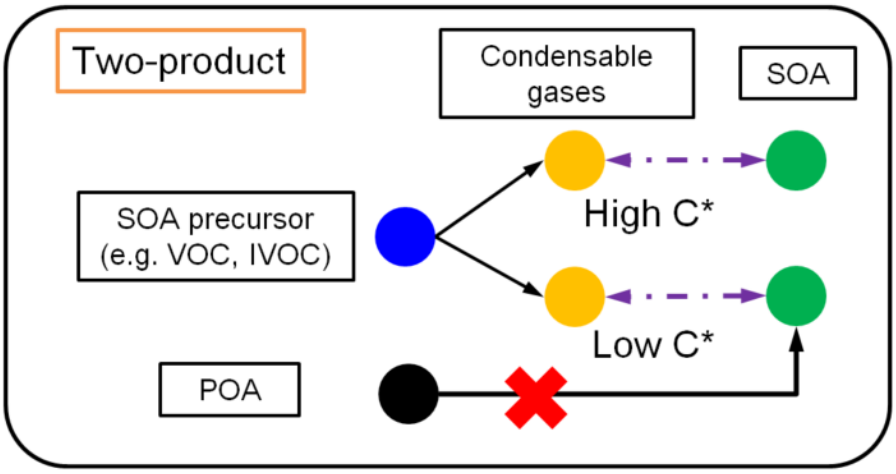

Figure 1 Illustration of a "two-product" SOA scheme combined with a non-volatile treatment of POA

The VBS framework (Donahue et al., 2006) expands the two-product model by having more condensable gases that are systematically organized by volatility (i.e., C^*). Condensable organic compounds are categorized based on their volatility into bins that are typically separated by a factor of 10, e.g., four bin with C^* of 1, 10, 100, 1000 μg/m^3:

$$\text{SOA precursor} + \text{OH} \rightarrow \alpha_1 \times \text{CG}|_{C^*=1} + \alpha_2\, \text{CG}|_{C^*=10} + \alpha_3 \times \text{CG}|_{C^*=100} + \alpha_4 \times \text{CG}|_{C^*=1000} \quad \text{R2}$$

Similar to the two-product model, the VBS framework is based on the absorptive partitioning theory and the CG yield (α) for each volatility bin can be obtained by fitting the results of laboratory studies. Many VBS schemes treat POA as being semi-volatile and able to dynamically partition between the gas and particle phase depending on environmental factors, similar to SOA. Figure 2 illustrates the

80 “1-dimensional” (1-D) VBS framework where volatility is the dimension that varies
81 (discretized to volatility bins) and panels a-d illustrate various treatments of SOA
82 aging. In the 2-D VBS introduced by Donahue et al. (2011), both volatility and
83 oxidation state can vary independently. The 1.5-D VBS introduced by Koo et al.
84 (2014) represents variations in volatility and oxidation state as a single coordinate by
85 assuming they are related.
86 Figure 2a depicts a four-bin VBS framework with no aging of OA after the initial
87 formation of SOA. Emitted SOA precursors (e.g., VOC, IVOC) undergo initial
88 gas-phase oxidation and produce four types of CGs which can immediately condense
89 to form SOA. Beyond initial oxidation, multi-generational aging processes can occur
90 and include functionalization and/or fragmentation of gas-phase CGs, oligomerization
91 of condensed-phase SOA, SOA photolysis, and heterogeneous SOA oxidation.
92 Functionalization and oligomerization typically increase SOA mass by lowering
93 volatility, whereas fragmentation and photolysis decrease SOA mass. Figure 2b
94 depicts a VBS framework incorporating a step-wise OH-oxidation functionalization
95 process as included in many VBS schemes, where CGs undergo gas-phase reactions
96 (usually parameterized as OH-oxidation) that add oxygen-containing functional
97 groups and successively lower volatility. This functionalization increases molecular
98 weight with each oxidation generation, which can be parameterized as a percentage
99 increase (usually 7.5% or 15%) to account for added oxygen (Robinson et al., 2007;
100 Shrivastava et al., 2015). Gas-phase reactions of CGs can cause molecular
101 fragmentation as well as functionalization. As SOA ages, fragmentation reactions may
102 gain significance (Cappa et al. 2012). Figure 2c shows a VBS framework with both
103 functionalization and fragmentation. In this scheme, OH-oxidation of the CGs forms
104 products across lower (due to functionalization) and higher (due to fragmentation)
105 volatility bins that are often parameterized using predefined fractions. Particle-phase
106 oligomerization, as illustrated by Figure 2d, is another SOA aging process where
107 condensed SOA molecules join together and form larger SOA molecules with
108 extremely low volatility. Some schemes refer to oligomerization as polymerization.

Typically, the rate of oligomerization is modeled as independent of the gas-phase oxidant level.

Given the diverse treatments of SOA formation employed in CTMs, it is both necessary and important to comprehensively understand and quantify the similarities and differences among schemes/models. Direct comparisons of simulated SOA concentrations across different CTMs can be both time-consuming and resource-intensive. Furthermore, variations in other model configurations, such as physical processes, may obscure the distinctions associated with the SOA schemes themselves. To address this issue, we performed offline calculations outside the selected CTMs to focus on SOA formation and aging processes, as described in Section 2. Details of each SOA model/scheme reviewed are presented in Section 3. Section 4 provides a comparative analysis of the non-aged SOA yields from typical precursors as simulated by each model/scheme. Furthermore, we explore how SOA aging is treated by different schemes and how NO*x* conditions impact SOA yields. Results from this study underscore the variability in SOA yields and highlight the need for careful consideration of model selection and application in the context of air quality studies.

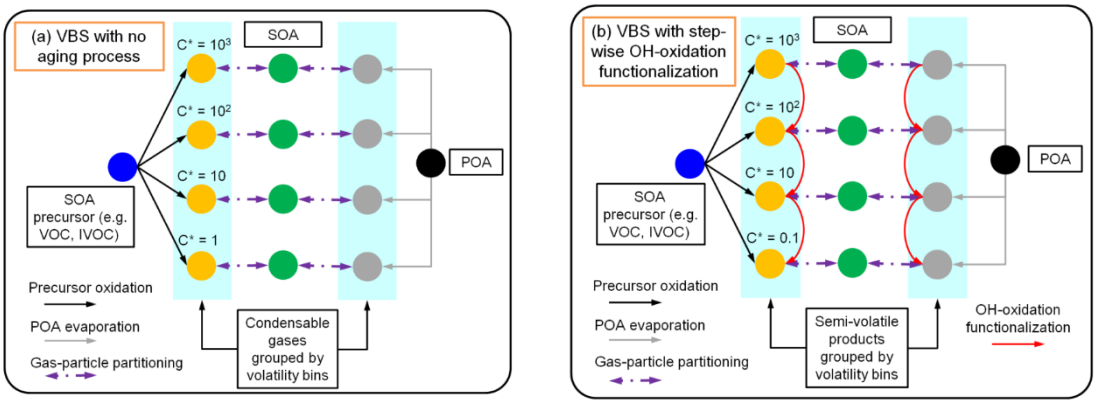

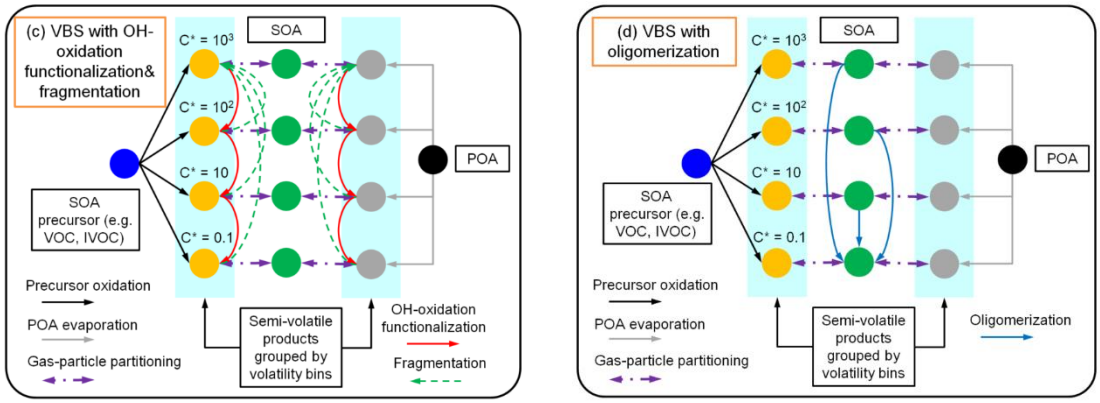

Figure 2 Illustration of VBS schemes with alternative treatments of aging: (a) no aging; (b) with step-wise OH oxidation causing functionalization only; (c) with OH-oxidation causing both functionalization and fragmentation; and (d) with condensed-phase oligomerization.

2. Methods

2.1 CTMs and SOA schemes reviewed

To understand the current state of SOA modelling in CTMs, we reviewed schemes implemented in several regional models that are used in the U.S., Europe, and Asia as well as one global model. We review eight SOA schemes implemented in five models, namely the Comprehensive Air Quality with Extensions (CAMx, https://www.camx.com/, accessed on Feb 15th, 2024), the Community Multiscale Air Quality (CMAQ, https://github.com/USEPA/CMAQ/, accessed on Feb 15th, 2024), GEOS-Chem (https://geos-chem.readthedocs.io/en/stable/, accessed on Feb 15th, 2024), WRF-Chem (https://ruc.noaa.gov/wrf/wrf-chem/, accessed on Feb 15th, 2024), and CHIMERE (https://www.lmd.polytechnique.fr/chimere/docs/, accessed on Feb 15th, 2024). For each model/scheme (hereafter "scheme" for simplicity), we reviewed the official documentation (e.g., user's guide), peer-reviewed publications, and, in some cases, the model source code to understand each SOA parameterization and gather parameter data. A comparative overview of the SOA schemes is presented in Table 1 while comprehensive details regarding their specific parameterizations can be found in Section S1 of the Supporting Information.

The review of these SOA schemes reveals diverse parameterizations ranging from simplified, non-volatile assumptions to complex, multi-dimensional volatility basis sets. CAMx offers two distinct approaches: the SOAP2 scheme (based on Strader et

al., 1999) and the 1.5-D VBS (Koo et al., 2014). SOAP2 has non-volatile POA and a two product SOA scheme (Figure 1) with yields fitted to the aged VBS scheme of Hodzic et al. (2016), effectively treating aging as implicit. The 1.5-D VBS treats POA as semi-volatile and explicitly models gas-phase aging for anthropogenic and intermediate volatility precursors via OH-oxidation (Figure 2b), although this stepwise aging is disabled for biogenic precursors to prevent aerosol mass overprediction. The CMAQ model also provides alternative schemes: the established AERO7 scheme (Appel et al., 2021) and the newer CRACMM scheme (Pye et al., 2023). AERO7 utilizes a 1-D VBS framework for POA and SOA that incorporates aging primarily through particle-phase processes (Figure 2d), specifically the oligomerization of anthropogenic and biogenic precursors and the hydrolysis of organic nitrates derived from monoterpenes. CRACMM also utilizes a 1-D VBS framework for POA and SOA and simulates aging through sequential gas-phase oxidation reactions involving functionalization and/or fragmentation (Figure 2c; Pye et al., 2023). GEOS-Chem includes a "Simple" scheme that treats SOA as non-volatile with fixed yields that are linked to ambient measurements, alongside a "Complex" 1-D VBS scheme without additional aging processes (Figure 2a; Pai et al., 2020). CHIMERE's 1-D VBS scheme is notable for its comprehensive aging scheme with functionalization, fragmentation, and oligomerization (Figure 2d) where oxidation products are redistributed across volatility bins (CHIMERE, 2023). The WRF-Chem MOSAIC scheme employs a 1-D VBS for most VOCs but applies a specific stepwise gas-phase aging mechanism exclusively to IVOCs (Shrivastava et al. 2011).

Despite these structural differences, the schemes share foundational similarities, particularly in the reliance on absorptive partitioning theory by most schemes. With the exception of the GEOS-Chem Simple scheme, which assumes irreversible condensation, all models utilize either a two-product or VBS framework to describe the equilibrium partitioning of semi-volatile organic compounds. However, the treatment of aging remains the most significant source of divergence. Approaches vary from neglecting aging entirely (GEOS-Chem Complex, CAMx SOAP2) to

implementing distinct mechanisms such as gas-phase oxidation (CAMx VBS, CMAQ CRACMM) versus particle-phase oligomerization (CMAQ AERO7). Additionally, the representation of IVOCs varies substantially, ranging from omission from the GEOS-Chem Simple scheme, a single lumped IVOC in most schemes, and several lumped IVOCs in the CRACMM scheme.

2.2 Offline calculation of non-aged SOA yields

The direct comparison of simulated SOA concentrations across different schemes through conducting full simulations is time-consuming and uncertain because configuring all models consistently is challenging. Furthermore, differences in the non-SOA physical and chemical processes between models may obscure the distinctions attributable specifically to the SOA schemes themselves. To address this issue, an offline calculation (Huang et al., 2023, 2024) is employed to compare the non-aged SOA yield (i.e., prior to any aging effects) associated with different precursors across various schemes. For a two-product scheme, the non-aged SOA yield (*Y*) is calculated by combing the gas-particle partitioning theory with the stoichiometric coefficients α_i:

$$Y = \frac{\alpha_1}{1 + C_1^*/C_{OA}} + \frac{\alpha_2}{1 + C_2^*/C_{OA}} \quad \text{Eq. 1}$$

where C_{OA} is the total ambient concentration of organic compounds (i.e., POA + SOA) and α_1, α_2, C_1^*, and C_2^* represent the stoichiometric coefficients and the effective saturation concentrations of the above two products, which is obtained by fitting the results of laboratory studies. Similarly, for a four-bin VBS scheme with no aging effects, the SOA yield is calculated as:

$$Y = \frac{\alpha_1}{1 + 1/C_{OA}} + \frac{\alpha_2}{1 + 10/C_{OA}} + \frac{\alpha_3}{1 + 100/C_{OA}} + \frac{\alpha_4}{1 + 1000/C_{OA}} \quad \text{Eq. 2}$$

where α_i is the non-aged oxidation yield for each volatility bin *i* (*i*=1,2,3,4). Utilizing either Eq. 1 or Eq. 2, the SOA yields under high- and low-NO*x* conditions can be determined at 298 K and total OA concentrations ranging from 0.1 μg/m^3 to 50 μg/m^3, using the stoichiometric coefficients provided by each scheme (see detailed parameters in Section S1 of the Supporting Information).

205

206 **Table 1** Summary of SOA schemes implemented in CTMs reviewed in this study[a]

SOA scheme	SOA precursors	Aging treatment	POA treatment	SOA photolysis
CAMx v7.20 *(Ramboll, 2022; Koo et al. 2014)*				
SOAP2	BENZ/TOL/XYL ISOP/TERP/SESQ	No aging effect	Non-volatile, no further reactions	Photolysis rate parameterized as 0.1% of the NO_2 photolysis rate (J_{NO2}).
1.5D VBS	IVOC	Gas-phase OH-oxidation aging for SOA formation from AVOC and IVOC	Semivolatile; gas-phase undergoes further oxidation	
CMAQ v5.4 *(Pye et al. 2023; https://github.com/USEPA/CMAQ)*				
AERO7	BENZ/TOL/XYL ISOP/TERP/SESQ IVOC	Particle-phase of semivolatile products forms oligomers; products generated by TERP + NO_3 undergo hydrolysis to form low-volatile products.	Semivolatile; gas-phase undergoes further oxidation	N/A
CRACMM	BENZ/TOL XYM/XYE APIN/LIM/SESQ IEPOX IVOC	OH oxidation aging resulting in functionalization and fragmentation based on modified 2-D VBS framework	Semivolatile; gas-phase undergoes further oxidation	N/A
GEOS-Chem v14.3.0 *(Pai et al. 2020; Pye et al. 2010; https://geos-chem.readthedocs.io/en/stable/)*				
Simple	ISOP/TERP/SESQ Anthropogenic precursor scaled based on CO emissions	No aging effect	Non-volatile; 50% of POA is directly emitted; 50% is formed with a lifetime of 1.15 days, without dependence on local oxidation levels.	Described in literature but not found in source code
Complex	BENZ/TOL/XYL IVOC ISOP/MTPO LIMO/SESQ		Semivolatile; gas-phase undergoes further oxidation with OH to form oxidized POA with lower volatility.	

SOA scheme	SOA precursors	Aging treatment	POA treatment	SOA photolysis
CHIMERE v2023 *(Zhang et al. 2013; Shrivastava et al. 2015; Couvidat et al. 2018; CHIMERE, 2023)*				
VBS	ARO1/ARO2 ALK4/ALK5 OLE1/OLE2 IVOC ISOP/TERP/ HUMULE	OH oxidation aging with both functionalization and fragmentation; aerosol phase undergoes oligomerization to form non-volatile products.	Semivolatile; gas-phase undergoes further oxidation.	N/A
WRF-Chem v4.4 *(Shrivastava et al. 2011)*				
MOSAIC	ALK4/ALK5 ARO1/ARO2 OLE1/OLE2 IVOC ISOP/TERP/SESQ	No aging for AVOC and BVOC; gas-phase OH-oxidation of IVOC with 15% of mass added for each generation; no fragmentation.	Semivolatile; gas-phase undergoes further oxidation	Described in literature (Zawadowicz et al. 2020) but turned off in source code

[a] See abbreviations in Supporting Information

The non-aged SOA yield Y is always calculated as mass-based in this study while the stoichiometric coefficients α_i could either be expressed in mass-base (g/g) or molar-base (ppm/ppm). An illustrative calculation is provided in the Section of S2 of the Supporting Information, with calculation spreadsheet publicly available (see Data Availability section). The non-aged SOA yields for CMAQ CRACMM are calculated slightly differently (details presented in Section S3 of the Supporting Information), given its special treatment of partially combining gas-phase chemistry and SOA formation. Our analysis included calculations for anthropogenic precursors (benzene, toluene, and xylene), IVOC and biogenic precursors (isoprene, monoterpene, and sesquiterpenes).

2.3 The effect of SOA aging

Some schemes, such as CAMx two-product and GEOS-Chem Simple, do not account for SOA aging while others adopt varying approaches to represent the aging process (for a comprehensive discussion, refer to Section 3). For schemes that include aging effects, we

calculated the aged SOA yields for each precursor at a given time *t* by summing over the particle fraction of all the relevant volatility bins (*i*) using Eq. 3:

$$\text{Aged SOA yields}|_t = \sum_n (f^i_{particle} \cdot \text{SOA mass}|^i_t) \quad \text{Eq. 3}$$

where $f^i_{particle}$ is the particle-phase fraction of each volatility bin (calculated based on Eq. 4) and $\text{SOA mass}|^i_t$ is the bin total SOA mass (gas-phase + particle-phase) at time *t*; *n* is the total number of bins.

$$f^i_{particle} = \frac{1}{1 + C^*_i / C_{OA}} \quad \text{Eq. 4}$$

For gas-phase OH-oxidation style aging (e.g., Figure 2b and 2c), the SOA mass is stepped through time ($\Delta t = t - (t\text{-}1)$) as follows:

$$\text{SOA mass}|^i_t = \text{SOA mass}|^i_{t\text{-}1} \times \left(f^i_{particle} + f^i_{gas} \cdot e^{-k_{OH}*[OH]*\Delta t}\right) + \sum_n [\text{SOA mass}|^k_{t\text{-}1} \times f^k_{gas} \cdot (1\text{-}e^{-k_{OH}*[OH]*\Delta t}) \times \alpha^i_k] \quad \text{Eq. 5}$$

The first term on the right hand side is the SOA mass in volatility bin (*i*) from the previous time step (*t-1*) multiplied by the fractions that remain after Δt in the particle-phase ($f^i_{particle}$) and gas-phase ($f^i_{gas} \cdot e^{-k_{OH}*[OH]*\Delta t}$; $f^i_{gas} = 1 - f^i_{particle}$) considering OH-oxidation. The second term is the SOA mass gain from OH-oxidation summed across all *n* volatility bins. Here, α^i_k is the mass yield coefficient from bin *k* to bin *i* and the term $f^k_{gas} \cdot (1\text{-}e^{-k_{OH}*[OH]*\Delta t})$ is the gas-phase fraction of SOA in bin *k* oxidized by OH during Δt.

For particle-phase oligomerization-style aging (e.g. Figure 2d and the CMAQ AERO7 scheme), the aged SOA yield includes the mass of a non-reactive and non-volatile oligomer bin (OLIG) in addition to the semi-volatile bins:

$$\text{Aged SOA yield}|_t = \sum_n (f^i_{particle} \cdot \text{SOA mass}|^i_t) + \text{SOA mass}|^{OLIG}_t \quad \text{Eq. 6}$$

The SOA mass (gas-phase + particle-phase) in each volatility bin (*i*) steps through time following Eq. 7 and the mass of the non-volatile oligomer bin ($\text{SOA mass}|^{OLIG}_t$) grows with mass-transfer from semi-volatile bins according to Eq. 8:

$$\text{SOA mass}|_t^i = S\text{OA mass}|_{t-1}^i \times (f_{gas}^i + f_{particle}^i \cdot e^{-k_{OLIG}*\Delta t}) \quad \text{Eq. 7}$$

$$\text{SOA mass}|_t^{OLIG} = S\text{OA mass}|_{t-1}^{OLIG} + \sum_n \{\text{SOA mass}|_{t-1}^i \cdot f_{particle}^i \cdot (1 - e^{-k_{OLIG}*\Delta t}) \cdot \beta^i\} \quad \text{Eq. 8}$$

240 k_{OLIG} is the oligomerization rate and β^i is the mass yield coefficient from bin *i* to the
241 non-volatile bin OLIG.
242 To compare the aging effects of different schemes, we applied Eq. 3 to Eq. 8 for one day of
243 aging with an OH concentration of 3×10^6 molecules/cm^3 with k_{OH} and/or k_{OLIG} for each
244 scheme when applicable. A time step (Δt) of 0.2 hr was used. Any additional calculations and
245 assumptions associated with each scheme are further described below.
246 **2.4 Box model tests based on different SOA schemes**
247 We implemented three updated SOA schemes in CAMx and performed 2-layer box modeling
248 of two locations with varied anthropogenic emissions to quantify how differences between
249 schemes can influence predicted SOA concentrations and their response to emission changes.
250 The alternate SOA schemes use the existing CAMx SOAP2 code with updated SOA yield
251 parameters so that model results clearly depend on yield assumptions rather than scheme
252 formulation or coding. Two regions of Texas were selected to capture contrasting emission
253 environments: Dallas-Fort Worth (DFW), a major urban area dominated by anthropogenic
254 emissions (e.g., aromatics and IVOCs), and Tyler (TYL), a rural area in Northeast Texas
255 characterized by high biogenic activity. The box model has a surface layer and a residual
256 layer with time-varying surface layer depth to provide a simple representation of pollutant
257 accumulation, carry-over, and diurnal variation. Simulations were conducted over a 5-day
258 period, utilizing meteorological inputs and initial conditions derived from the Texas
259 Commission on Environmental Quality (TCEQ) 2019 3-D CAMx modeling platform (TCEQ,
260 2022).
261 We implemented three new SOA schemes into CAMx that emulate SOA yields produced by
262 the CMAQ AERO7, CMAQ CRACMM and Simple schemes. Each scheme was implemented
263 by updating the yield parameters used by the CAMx SOAP2 scheme. For the CMAQ AERO7
264 and CRACMM schemes, yield curves were fitted to the respective data (Figure S3) for each

SOA precursor. These yields were mapped to the volatility bins defined by CAMx SOAP2 to obtain the corresponding molar-based stoichiometric coefficients (Table S11-S14). Like the GEOS-Chem Simple scheme, the CAMx Simple scheme treats SOA as non-volatile with fixed yields that are based on multi-model averages and work by Seltzer et al. (2021). Detailed descriptions of the fitting procedures, updated Simple yields, and box model configurations are provided in the Section S3 of the Supporting Information.

We further investigate the response of SOA concentrations to varying anthropogenic VOC and NO*x* emissions by performing a matrix of 100 simulations for each location and SOA scheme. This approach allows for a comparison of scheme performance across a wider range of atmospheric concentrations and VOC/NO*x* ratios. Anthropogenic emissions in the sensitivity runs were based on weekday rates, while the biogenic emissions remained unscaled and varied by date, consistent with the base case simulations. Anthropogenic VOC emissions were scaled from 0.1 to 1.0 (in increments of 0.1), while anthropogenic NO*x* emissions were scaled from 0 to 9 (in increments of 1) which caused oxidant production to transition between NO-limited and VOC-limited conditions. An additional simulation with a 50% reduction in NO*x* emissions was conducted to examine SOA response to NO*x* abatement, which is a critical consideration for current and future air quality planning.

3. Results

3.1 Comparison of non-aged SOA yields

Non-aged SOA mass yields (g/g) for all schemes (except CMAQ CRACMM) are summarized in Table 2. Non-aged refers to the yields immediately following precursor oxidation and before any subsequent SOA aging process. Since mass yields can vary with C_{OA}, we assume C_{OA} of 10 μg/m^3 in Table 2, which is relevant to ambient air quality and often used as a reference C_{OA} for SOA yield comparisons. The ratio of maximum to minimum non-aged SOA yields for a same precursor shows wide variations across different schemes, with the least variation (factor of 1.8) observed for monoterpene at low NO*x* conditions and over three orders of magnitude for IVOC (factor of 3715). These variations can become greater when C_{OA} is either increased or decreased from 10 μg/m^3 (as assumed for

293 Table 2) and when effects of aging processes on non-aged yields are included (as shown in
294 Section 4.2).
295 3.1.1 Non-aged SOA yields from anthropogenic VOC
296 Figure 3 shows how the non-aged SOA mass yields depend on C_{OA} for three anthropogenic
297 VOC (AVOC), namely benzene (BENZ), toluene (TOL), and xylene (XYL). For WRF-Chem
298 and CHIMERE, the SOA yields for model species ARO1 are used to represent BENZ and
299 TOL whereas those of ARO2 are used for XYL. As illustrated by Figure 3, the SOA yields
300 from aromatics generally increase with C_{OA}, except for GEOS-Chem Simple. The SOA
301 yields become independent of C_{OA} when the product is treated as non-volatile as exemplified
302 by the GEOS-Chem Simple scheme, which assumes constant SOA yields of 100% for all
303 three precursors. Conversely, the SOA yields increase strongly with C_{OA} when the SOA is
304 treated as semi-volatile. The CAMx SOAP2 scheme is an intermediate case with SOA yields
305 increasing more gradually with C_{OA} than the CHIMERE scheme. CMAQ AERO7 and
306 GEOS-Chem Complex predict almost identical SOA yields (due to close stoichiometric
307 coefficients) and exhibit no dependence on C_{OA} under low NO*x* conditions. Overall, schemes
308 consistently show higher ASOA yields from aromatics under low NO*x* than high NO*x*
309 conditions but diverge in the magnitude of these yields (max./min. yields at 10 $\mu g/m^3$ ranging
310 from 2.0 to 5.8) and diverge in how yields depend on C_{OA} (ranging from independent to
311 strongly increasing).

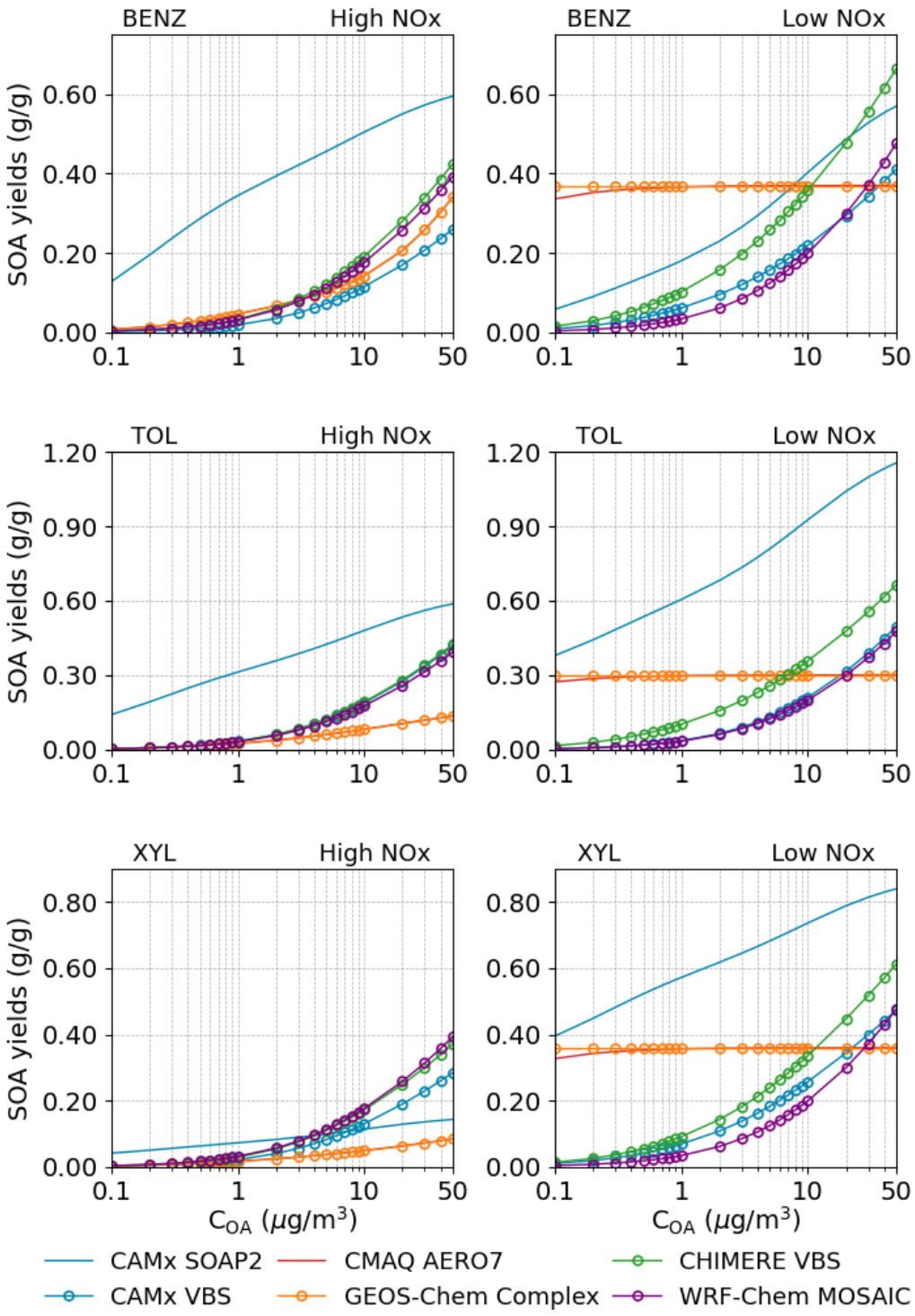

Figure 3 Comparison of the non-aged SOA yields (g/g) as functions of C_{OA} for three anthropogenic VOC among different schemes (CMAQ CRACMM not included). SOA yields are calculated at 298 K. Note that y-axis scales vary by precursor to highlight scheme discrepancies across different yield magnitudes.

317 **Table 2** Non-aged SOA yields (g/g) for different precursors across schemes at 298 K and C_{OA}
318 of 10 μg/m^3.

Precursor-NOx case	CMx[1] SP2	CMx VBS	CMQ AE7	CMQ CRM	G-C Spl	G-C Cpx	CMR VBS	W-C MOS	Avg[7]	Max/Min[8]
BENZ[2]-high	0.51	0.12	0.14	0	/	0.14	0.19	0.18	0.21	4.4
BENZ-low	0.40	0.22	0.37	0	/	0.37	0.36	0.20	0.32	2.0
TOL[3]-high	0.48	0.19	0.08	0	/	0.08	0.19	0.18	0.20	5.8
TOL-low	0.93	0.21	0.30	0	/	0.30	0.36	0.20	0.38	4.6
XYL[4]-high	0.11	0.13	0.05	0	/	0.05	0.17	0.18	0.12	3.6
XYL-low	0.74	0.26	0.36	0	/	0.36	0.34	0.20	0.38	3.7
IVOC[5] high	0.36	0.51	1.00	0	/	0.20	2.7×10^{-4}	2.7×10^{-4}	0.35	3715
IVOC-low	0.55	0.51	1.00	0	/	0.73	2.7×10^{-4}	2.7×10^{-4}	0.46	3715
ISOP-high	0.05	0.01	0.05	0	0.03	0.04	0.04	0.01	0.03	4.0
ISOP-low	0.09	0.03	0.05	0	0.03	0.04	0.07	0.02	0.05	3.8
TERP-high	0.14	0.09	0.17	0	0.10	0.09	0.13	0.10	0.12	1.8
TERP-low	0.21	0.18	0.17	0	0.10	0.19	0.25	0.18	0.18	2.5
SESQ[6]-high	0.52	0.22	0.44	0	0.10	0.84	0.20	0.22	0.36	8.4
SESQ-low	0.70	0.22	0.44	0	0.10	0.42	0.20	0.22	0.33	7.0

319 [1] Model name abbreviations are CMx for CAMx, CMQ for CMAQ, G-C for GEOS-Chem, CMR for
320 CHIMERE, and W-C for WRF-Chem. Scheme name abbreviations are SP2 for SOAP2, AE7 for AERO7, Spl
321 for Simple, Cpx for Complex, and MOS for MOSAIC.
322 [2] For WRF-Chem and CHIMERE, results for BENZ are based on ARO1.
323 [3] For WRF-Chem and CHIMERE, results for TOL are based on ARO1.
324 [4] For WRF-Chem and CHIMERE, results for XYL are based on ARO2. For CMAQ CRACMM, results for
325 XYL are averages of XYE and XYM.
326 [5] For CMAQ CRACMM, IVOC yields are average of alkane and oxygenated IVOCs (see details in Table S17).
327 For WRF-Chem MOSAIC, IVOC is assumed to have 50% oxygen.
328 [6] For CHIMERE, results for SESQ are based on humulene.
329 [7] Multi-model average yield excluding GEOS-Chem Simple for aromatics and IVOC, and excluding CRACMM
330 for ISOP.
331 [8] Ratio of maximum to minimum yield.

3.1.2 Non-aged SOA yields from biogenic VOC

Figure 4 shows how the non-aged SOA mass yields depend on C_{OA} for three biogenic VOC (BVOC), namely isoprene (ISOP), monoterpenes (TERP), and sesquiterpenes (SESQ). For isoprene, CMAQ includes heterogeneous SOA formation from IEPOX (Pye et al., 2013), which is outside the scope of this evaluation and thus is not discussed in this study.

Overall, the BSOA yield patterns closely resemble those of ASOA. All schemes, except for GEOS-Chem Simple, predict an increase in yields associated with C_{OA}. However, the magnitude of SOA yields varies significantly across schemes, ranging from 1.8 to 8.4 under high NO*x* conditions and 2.5 to 7.0 under low NO*x* conditions. Additionally, model predictions regarding the influence of NO*x* on BSOA yields are inconsistent, with some indicating an increase, others a decrease, and some showing no effect. For instance, SOA yields from ISOP under high NO*x* conditions, as simulated by two CAMx schemes, WRF-Chem MOSAIC, and CHIMERE VBS, are approximately half of those under low NO*x* conditions. In contrast, CMAQ AERO7 and GEOS-Chem schemes suggest that SOA yields are independent of NO*x* levels. Regarding TERP-derived SOA, all schemes, except for CMAQ AERO7 and GEOS-Chem Simple, predict more than 50% higher yields under low NO*x* conditions compared to high NO*x* conditions. The latter two schemes show no difference between NO*x* regimes. For SESQ, four models (CAMx VBS, CMAQ AERO7, CHIMERE VBS, and WRF-Chem MOSAIC) predict no distinction in SOA yields between high and low NO*x* conditions. Conversely, CAMx SOAP2 suggests higher yields under low NO*x* conditions, whereas the GEOS-Chem Complex scheme predicts the opposite.

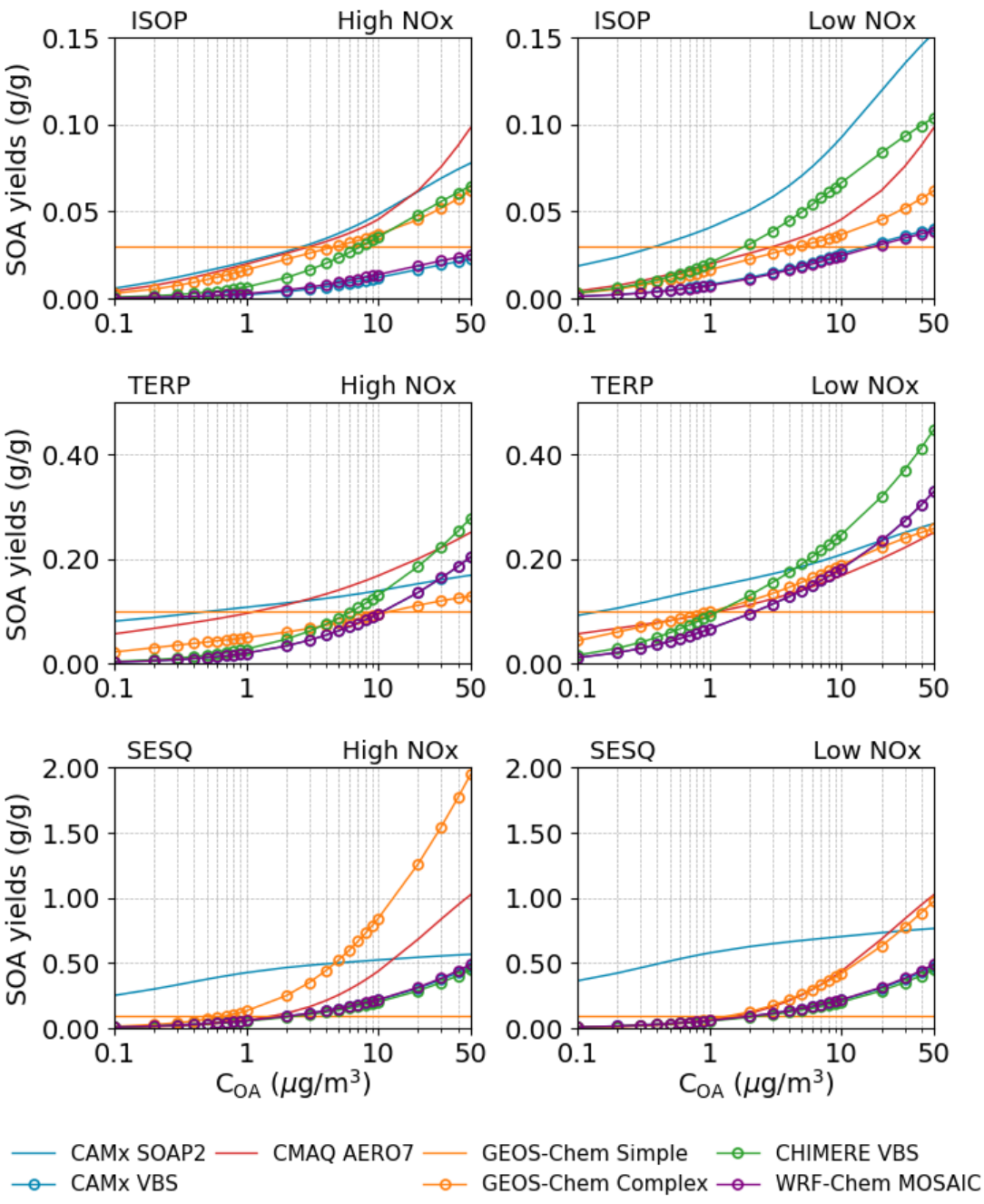

353

354 **Figure 4** Comparison of the non-aged SOA yields (g/g) as functions of C_{OA} for three
355 biogenic VOC among different schemes (CMAQ CRACMM not included). SOA yields are
356 calculated at 298 K. Note that y-axis scales vary by precursor to highlight scheme
357 discrepancies across different yield magnitudes.

358 3.1.3 Non-aged SOA yields from intermediate volatility organic compounds (IVOC)

359 IVOC emissions make important contributions to ASOA formation (Zhao et al., 2016; Ma et
360 al., 2016; Zhao et al., 2014). The SOA yields from IVOC, referred to as IV-SOA, predicted
361 by each scheme are shown in Figure 5. The GEOS-Chem Simple scheme is omitted since it

does not explicitly account for IVOC. Additionally, the results for CMAQ CRACMM are discussed separately in Section 4.2.3, due to its distinct treatment of several IVOC types.

SOA yields from IVOC in the CAMx VBS scheme shows a strong positive dependence on C_{OA} whereas CAMx SOAP2 and GEOS-Chem Complex exhibit much weaker responses. Constant SOA yields of 1.0 g/g are set in CMAQ AERO7, regardless of NO*x* levels, surpassing the values predicted by other schemes. SOA formation from IVOC in CHIMERE VBS and WRF-Chem MOSAIC is treated as multi-generational oxidation (R13-R18 in Supplementary Information), resulting in extremely low non-aged SOA yields (<0.001 g/g).

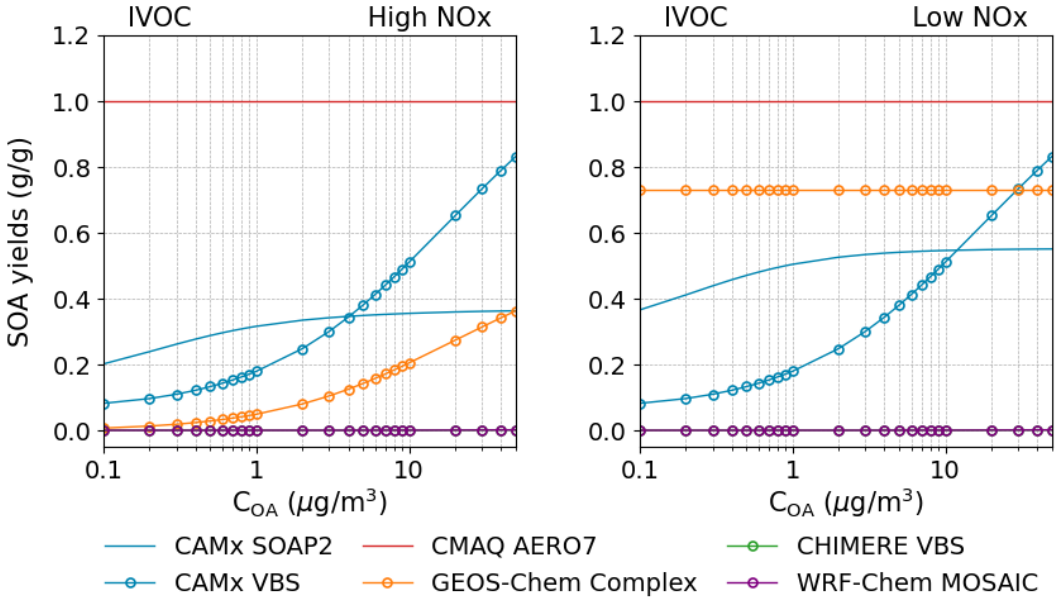

Figure 5 Comparison of the non-aged SOA yields (g/g) as functions of C_{OA} for IVOC among different schemes (CMAQ CRACMM and GEOS-Chem Simple not included). SOA yields are calculated at 298 K.

3.2 Comparison of SOA aging

Among the eight schemes we evaluated, the CAMx SOAP2, GEOS-Chem Simple, and GEOS-Chem Complex schemes do not incorporate explicit SOA aging processes. However, the SOAP2 yields are derived from a VBS parameterization that includes aging (Hodzic et al., 2016) and may therefore be considered pre-aged (Emery et al., 2024). The remaining schemes account for SOA aging using one or more of three mechanisms: gas-phase OH-oxidation, condensed-phase oligomerization, and condensed-phase hydrolysis. Gas-phase OH-oxidation aging is typically parameterized as functionalization reactions that generate

less volatile products (e.g. Figure 2b) and/or fragmentation reactions that produce more volatile products (e.g. Figure 2c). This mechanism is adopted in CAMx VBS (for AVOC and IVOCs only), CMAQ CRACMM, WRF-Chem MOSAIC and CHIMERE VBS, with implementation being specific to each scheme. Condensed-phase oligomerization aging (e.g. Figure 2d) is characterized as a first-order particle-phase reaction, usually assuming a lifetime of 30 hr, leading to non-volatile product formation independent of oxidant concentrations. CMAQ AERO7 applies this process for SOA formed from all precursors except monoterpenes. For SOA derived from NO_3 oxidation of monoterpenes, AERO7 instead applies condensed-phase hydrolysis, yielding non-volatile products with a lifetime of ~3 hr.

To compare the aging effects on SOA yields across different schemes, we assumed a 24-hour exposure to an OH concentration of 3×10^6 molecules/cm^3 (equivalent to 2.6×10^{11} molecules·s·cm^{-3}) for the OH-oxidation aging process or a 24-hour of condensed-phase oligomerization/hydrolysis when calculating the aged SOA yields (details presented below). Table 3 summarizes the aged SOA yields (when applicable) at 298 K with a C_{OA} of 10 μg/m^3 as simulated by each scheme. Figure 6 and Figure 7 further compare the non-aged and aged SOA yields for each scheme and SOA precursor, while Figure 8 separately illustrates the aging effects on IVOC-derived SOA across different schemes.

3.2.1 Aging in CAMx VBS

The CAMx VBS scheme incorporates step-wise gas-phase OH-oxidation aging for AVOC and IVOC without accounting for fragmentation processes (Figure 2b). The calculation of aged SOA yields follows Eq. 3 to Eq. 5, using a k_{OH} value of 2×10^{-11} cm^3 molecule^{-1} s^{-1} and an OH concentration of 3×10^6 molecules cm^{-3}. Figure 7a-b illustrates how SOA yields change as a function of accumulated OH exposure under high and low NO*x* conditions for different precursors. In the CAMx VBS scheme, SOA yields increase with OH exposure though the rate of aging slows as the OH exposure increases. With a 24-hour period (corresponding to an OH exposure of 2.6×10^{11} molecules·s·cm^{-3}), SOA yields from aromatics increase by a factor of 5-6 under high NO*x* conditions and 3-5 under low NO*x* conditions compared to their non-aged yields. For IVOC, aged SOA yields increase by 125% relative to

the non-aged yields (Figure 8b). These findings highlight the significant influence of aging processes implemented in the CAMx VBS scheme.

Table 3 Aged SOA yields (g/g) for different precursors across schemes at 298 K and C_{OA} of 10 μg/m^3. Shaded values indicate no aging effect (i.e. identical to values in Table 2).

Precursor-NOx case	CMx[1] SP2	CMx VBS	CMQ AE7	CMQ CRM	G-C Spl	G-C Cpx	CMR VBS	W-C MOS	Avg[7]	Max/Min[8]
BENZ[2]-high	0.51	0.80	0.22	0.23	/	0.14	0.79	0.18	0.41	5.6
BENZ-low	0.40	1.07	0.37	0.67	/	0.37	1.11	0.20	0.60	5.6
TOL[3]-high	0.48	1.30	0.12	0.11	/	0.08	0.79	0.18	0.44	15.7
TOL-low	0.93	1.33	0.30	0.50	/	0.30	1.11	0.20	0.67	6.7
XYL[4]-high	0.11	0.83	0.07	0.09	/	0.05	0.66	0.18	0.29	16.9
XYL-low	0.74	1.14	0.36	0.51	/	0.36	0.98	0.20	0.61	5.7
IVOC[5] high	0.36	1.15	1.00	0.31	/	0.20	0.02	1.20	0.60	73.7
IVOC-low	0.55	1.15	1.00	0.53	/	0.73	0.02	1.20	0.74	73.7
ISOP-high	0.05	0.01	0.06	/	0.03	0.04	0.08	0.01	0.04	6.8
ISOP-low	0.09	0.03	0.06	/	0.03	0.04	0.12	0.02	0.06	5.0
TERP-high	0.14	0.09	0.17	0.84	0.10	0.09	0.54	0.10	0.26	5.7
TERP-low	0.21	0.18	0.17	0.20	0.10	0.19	0.80	0.18	0.25	17.5
SESQ[6]-high	0.52	0.22	0.78	0.54	0.10	0.84	0.86	0.22	0.51	8.6
SESQ-low	0.70	0.22	0.78	1.04	0.10	0.42	0.86	0.22	0.54	10.4

[1] Model name abbreviations are CMx for CAMx, CMQ for CMAQ, G-C for GEOS-Chem, CMR for CHIMERE, and W-C for WRF-Chem. Scheme name abbreviations are SP2 for SOAP2, AE7 for AERO7, Spl for Simple, Cpx for Complex, and MOS for MOSAIC.

[2] For WRF-Chem and CHIMERE, results for BENZ are based on ARO1.

[3] For WRF-Chem and CHIMERE, results for TOL are based on ARO1.

[4] For WRF-Chem and CHIMERE, results for XYL are based on ARO2. For CMAQ CRACMM, results for XYL are averages of XYE and XYM.

[5] For CMAQ CRACMM, IVOC yields are average of alkane and oxygenated IVOCs (see details in Table S17). For WRF-Chem MOSAIC, IVOC is assumed to have 50% oxygen.

[6] For CHIMERE, results for SESQ are based on humulene.

[7] Multi-model average yield excluding GEOS-Chem Simple for aromatics and IVOC, and excluding CRACMM for ISOP.

[8] Ratio of maximum to minimum yield.

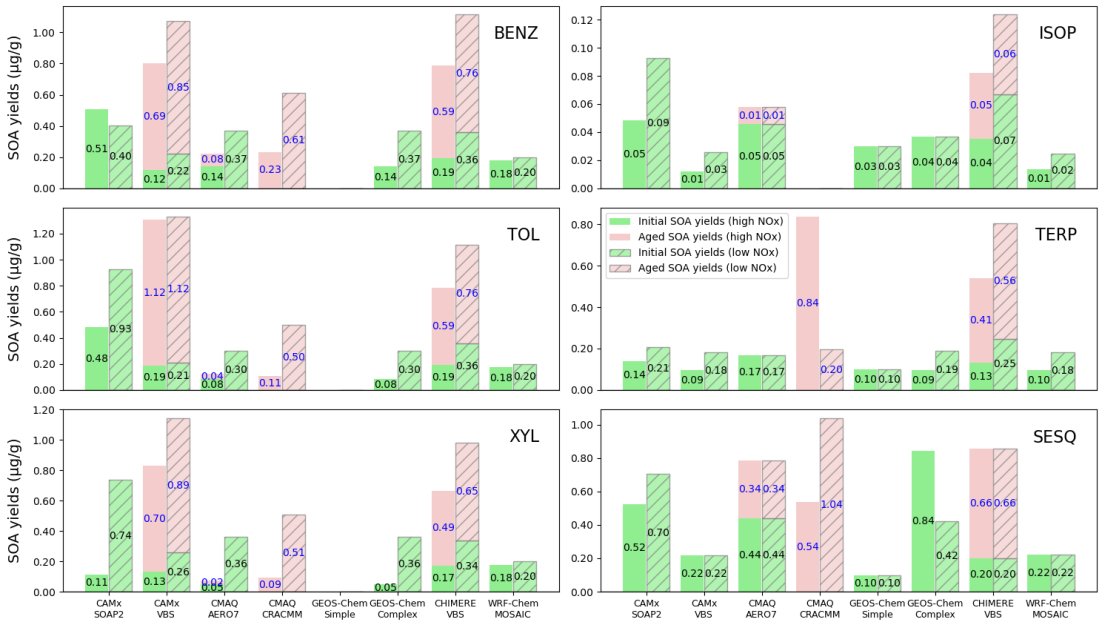

Figure 6 Effect of aging on SOA yields (g/g) for different precursors under high and low NO*x* conditions. Note that y-axis scales vary by precursor to highlight scheme discrepancies across different yield magnitude.

3.2.2 Aging in CMAQ AERO7

The SOA aging process in the CMAQ AERO7 scheme involves particle-phase oligomerization (Figure 2d) and hydrolysis. Oligomerization applies to SOA formed from ISOP, SESQ, and aromatics (only under high-NO*x* conditions) while hydrolysis affects SOA formed from monoterpenes oxidation by NO_3 radical. The aged SOA yields resulting from oligomerization and hydrolysis follows Eq. 6 to Eq. 8, with rate constants $k_{OLIG} = 9.49\times10^{-6}\ s^{-1}$ and $k_{hydro} = 9.26\times10^{-5}\ s^{-1}$. Figure 7b illustrates the evolution of SOA yields over 24 hours of oligomerization, showing increases of 27%, 79%, and 46%-57% for ISOP, SESQ, and aromatics, respectively. This increase results from the reduced volatility of SOA due to oligomerization. The hydrolysis reaction, assuming a shorter lifetime of approximately 3 hr, leads to a 48% increase in SOA yield from monoterpene-derived organic nitrates over 1 day. Although the hydrolysis rate is nearly ten times faster than that of oligomerization, the overall yield increase is moderated because the hydrolysis products have lower molecular weights than their parent compounds.

3.2.3 Aging in CMAQ CRACMM

The aging processes in CMAQ CRACMM involve the gas-phase OH-oxidation reactions of secondary oxygenated L/S/IVOCs, leading to both fragmentation and functionalization, and resulting in products with varying volatilities. As illustrated in Figure 7e-f, the impact of aging on SOA yields depends on the precursor and varies between high NO*x* and low NO*x* conditions. Under high NO*x* conditions, SOA yields from all precursors increase substantially during the first 6-8 hours, after which the growth rate becomes negligible (except for TERP, which continues to increase). After 24 hours of aging, SOA yields under high NO*x* conditions range from 0.093 g/g for XYL to 0.838 g/g for TERP (Table 3). In contrast, under low NO*x* conditions, all precursors show a sharp increase in SOA yields within the first 30 mins. Subsequently, SOA yields from XYL begin to decline, gradually reaching a minimum value of approximately 0.511 g/g after 16 hours. On the contrary, BENZ yields continue to increase slightly, peaking around 0.670 g/g. TERP, TOL, and SESQ yields exhibit minimal change after their initial increase. After 24 hours, SOA yields under low NO*x* conditions range from 0.195 g/g for TERP to 1.039 g/g for SESQ.

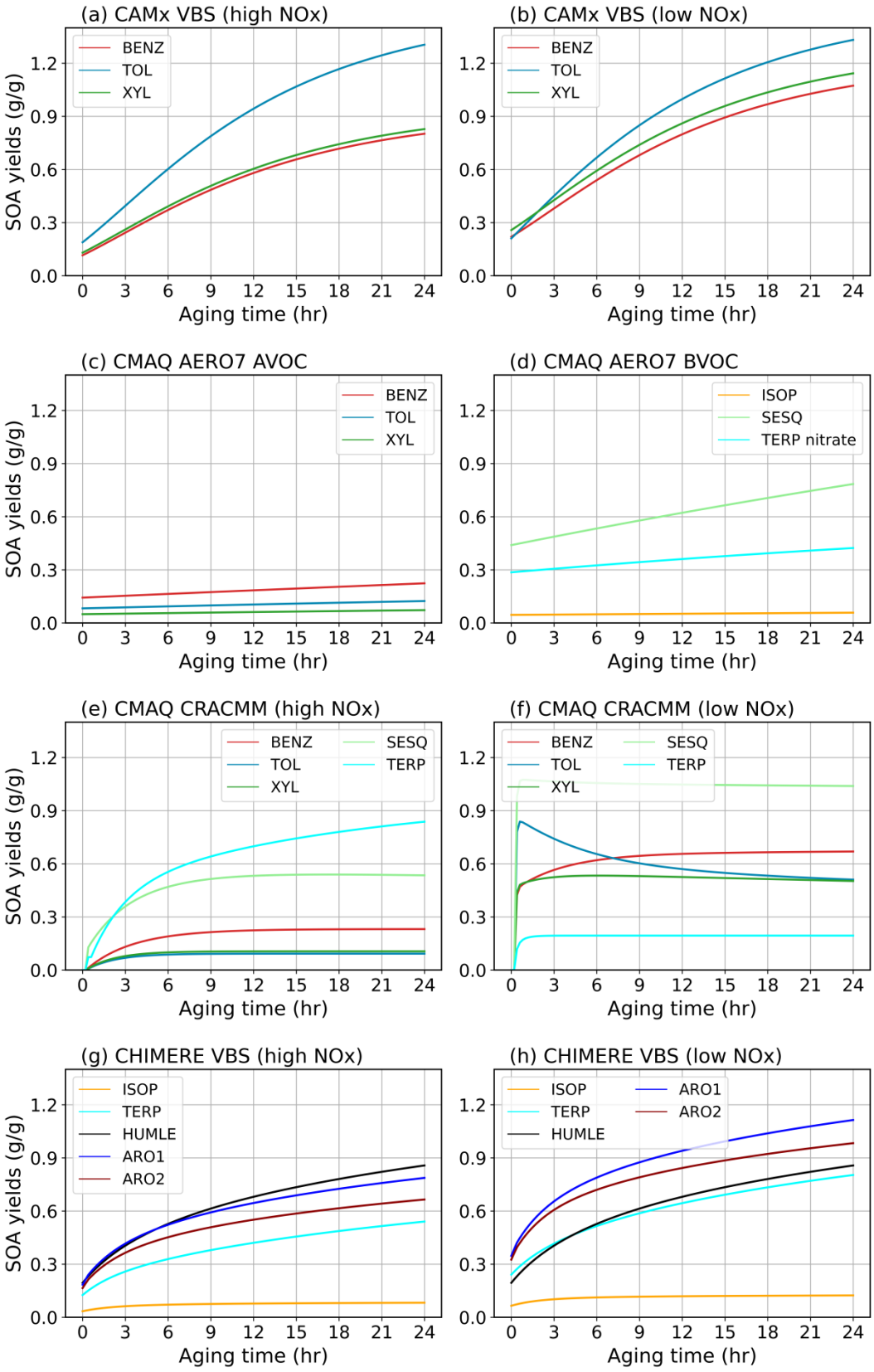

Figure 7 Effect of aging on SOA yields (g/g) from different precursors as a function of OH exposure or aging time in different schemes. (a-b) CAMx VBS; (c-d) CMAQ

AERO7; (e-f) CMAQ CRACMM; and (g-h) CHIMERE VBS. The numbers in the brackets indicate the relative change of SOA yields at hour 24 to hour 0.

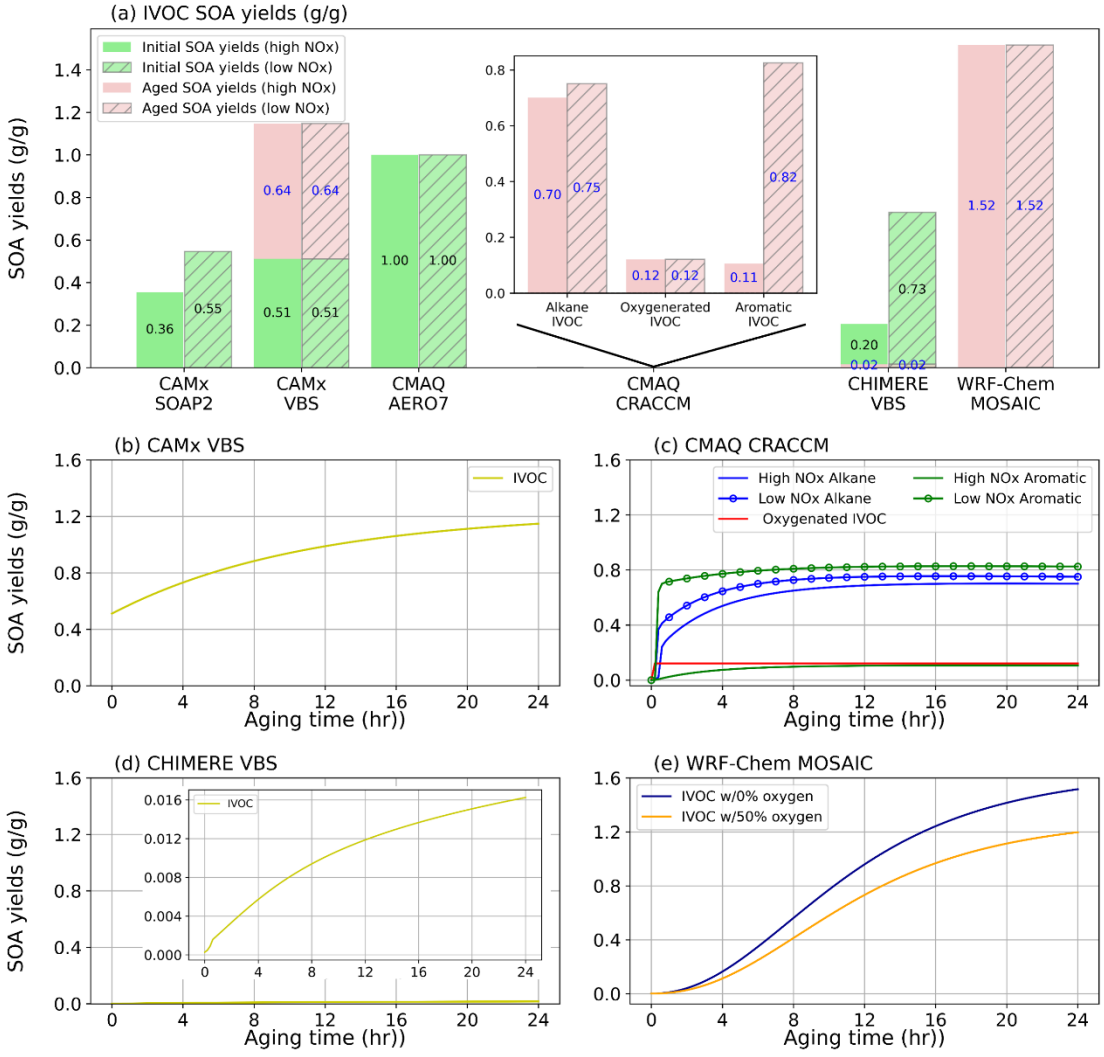

Figure 8 Effect of aging on SOA yields (g/g) for IVOC precursors under high and low NO*x* conditions for different schemes.

Unlike other schemes, the CMAQ CRACMM scheme classifies IVOC into alkanes, aromatics, and oxygenated IVOC based on their functional groups. Emitted oxygenated IVOC do not exhibit aging effects, as their oxidation products are assumed to be non-volatile (Figure 8c). In contrast, SOA yields from alkane and aromatic IVOC increase with the aging time, with the growth rate becoming negligible after approximately 10 hours. SOA yields from oxygenated IVOC (0.121 g/g) are independent of NO*x* conditions. The other two IVOC types show higher SOA yields under low NO*x* conditions, particularly for aromatic IVOC, where the SOA

yields under low NOx conditions (0.825 g/g) are nearly 8 times that under high NO*x* conditions (0.105 g/g).

3.2.4 Aging in CHIMERE VBS

The CHIMERE VBS scheme accounts for aging through gas-phase functionalization and fragmentation, as well as condensed-phase oligomerization, as shown in Supplementary Information R9 to R12. Figure 7d presents the combined aging effects on SOA over a 24-hour period under this scheme. Among BVOC, the aging effect is more pronounced for TERP and humulenes (HUMULE) than for ISOP. Under high NO*x* conditions, the SOA yields from ISOP, TERP, and HUMULE increase by 141%, 331%, and 341%, respectively, over one day. In contrast, under low NO*x* conditions, the aging effect is generally less significant, except for HUMULE, which exhibits a similar level of aging under both NO*x* regimes. Aromatics show substantial increase in SOA yields—over 300% under high NO*x* and 200% under low NO*x* conditions.

Aging of SOA from IVOC results in a dramatic increase in yields—by nearly a factor of 60 within one day, as shown by Figure 8d. However, the absolute SOA yields from IVOC remain low (approximately 0.01 g/g), which is attributed to the non-aged low SOA formation ($\sim 10^{-4}$ g/g) and the dominance of fragmentation at higher oxidation generations. From the third oxidation generation onward, 75% of the condensable gases undergo fragmentation into more volatile products, while only 15% undergo functionalization, as described in Supplementary Information R14.

3.2.5 Aging in WRF-Chem MOSAIC

The WRF-Chem MOSAIC scheme does not include SOA aging processes for AVOC and BVOC. SOA formation from IVOC is parameterized as a stepwise gas-phase OH-oxidation process. For the non-oxygen component of condensable gases, a 15% mass gain is assumed for each generation (as per Supplementary Information R15 and R16). Meanwhile, the oxygenated component shifts to lower volatility bins without mass gain (as per Supplementary Information R17 and R18). The scheme does not consider fragmentation or condensed-phase oligomerization. Figure 8e illustrates aging effects under two scenarios: IVOC with hydrocarbon-like characteristics (0%

oxygen by mass at t=0, representing of diesel emissions) and IVOC with 50% oxygen by mass (representing of biomass burning emissions). In both cases, the non-fragmenting stepwise aging process in WRF-Chem results in substantial increases in SOA yields. At an OH exposure of 2.6×10^{11} molecule·s·cm^{-3} (i.e. a 24-hour period), SOA formed from hydrocarbon-like IVOC exceeds 1 g/g, despite an initially negligible yield.

3.3 NO*x* effects on SOA yields

Evaluating SOA yields for seven precursor types across eight modeling schemes results in 56 potential characterizations of how NO*x* levels influence SOA formation. Table S18 and S19 present the ratios of non-aged and aged SOA yields under high and low NO*x* conditions. For non-aged SOA yields, 11 of the 56 cases are missing and 14 cases are designed to exhibit no NO*x* dependence, leaving 31 meaningful comparisons. Among these, 29 cases show lower SOA yields under high NO*x* conditions. For aged SOA yields, 5 cases are missing and 14 are designed with no NO*x* effect, leaving 37 meaningful comparisons, of which 34 also show lower SOA yields under high NO*x* conditions. These results indicate a general trend of higher SOA yields under low NO*x* conditions, although a few exceptions are observed. In some cases, the NO*x* effect is reversed—that is, SOA yields are higher under high NO*x* conditions than under low NO*x* conditions. This is seen for BENZ in the CAMx SOAP2 scheme, TERP in CMAQ CRACMM, and SESQ in the GEOS-Chem Complex scheme. The NO*x* effect on terpene-derived SOA in CRACMM is particularly noteworthy: the model predicts an eightfold increase in SOA yields under high NO*x* conditions compared to low NO*x*. This is significant given that terpenes are key SOA precursors in many forested regions, such as the Eastern U.S., where anthropogenic NO*x* emissions may change due to ongoing urban development (which could increase NO*x* levels) or the implementation of emission control technologies (which may reduce them). Experimental studies, including those by Sarrafzadeh et al. (2016) and Wildt et al. (2014), have consistently found that terpene-derived SOA yields are higher under low NO*x* conditions, a result that aligns with most of the evaluated schemes but

contrasts with the predictions made by CRACMM.

3.4 SOA variations in box model simulations

The box model simulations reveal significant discrepancies in predicted SOA concentration and composition among the selected schemes at both the urban (DFW) and rural (TYL) locations (Figure 9). The total SOA concentrations can vary by a factor of 2–3 between schemes even under identical meteorological and emission inputs. Overall, SOA concentrations are higher at DFW than at TYL. At both locations, all schemes exhibit a consistent diurnal profile characterized by SOA accumulation throughout the day and night, followed by a sharp decline in the early morning (beginning around 06:00 LST) caused by expansion of the planetary boundary layer (PBL). At DFW, the temporal trends are similar across the four schemes; however, the magnitude varies, with Simple and AERO7 predicting the highest concentrations, while CRACMM predicts the lowest. At TYL, the inter-model spread is narrower than at DFW. Notable differences in diurnal dominance emerge: SOAP2 and CRACMM predict the highest concentrations overnight—a pattern distinct from DFW—while Simple and CRACMM produce the highest values during daytime hours. Figure 9c-d shows the maximum and minimum average SOA concentrations. At DFW, Simple and CRACMM predict the highest and lowest total SOA concentrations, respectively. Conversely, at TYL, CRACMM predicts the highest average concentration, while AERO7 predicts the lowest.

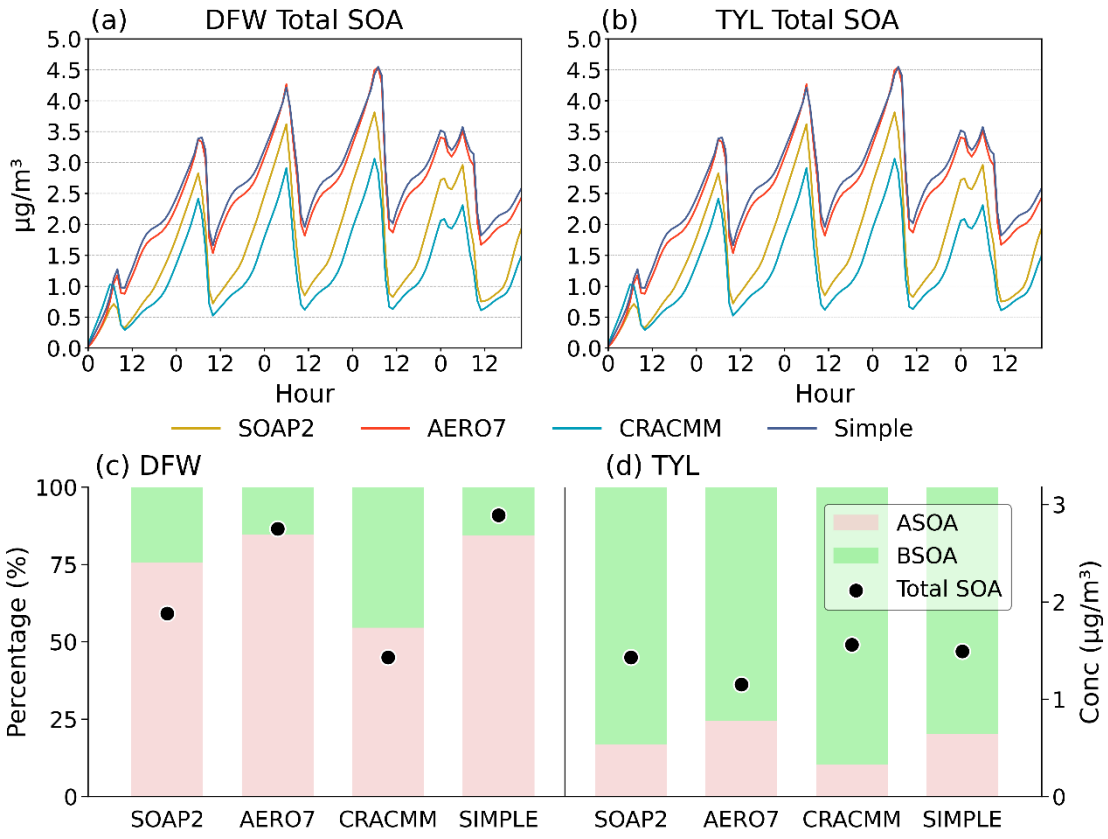

Figure 9 Diurnal profiles of total SOA (µg/m^3) from the 5-day box model base simulations at (a) DFW and (b) TYL. Average SOA concentrations (µg/m^3) averaged over days 2 through 5 of base model simulations for each SOA scheme (circles) and average contributions of ASOA and BSOA (bars)

Response surface plots for 24-hour average SOA concentrations derived from the matrix of simulations with varied anthropogenic NO*x* and VOC emissions are presented in Figure S4-S5. At DFW, total SOA concentrations generally decrease as anthropogenic NO*x* emissions increase relative to the base case (scaling factors 2–9) for all schemes, with the notable exception of CRACMM. CRACMM predicts negligible changes or a slight increase in SOA as NO*x* rises from low to mid scaling factors and a decrease is observed only when NO*x* emissions are increased by about a factor of 7 or greater. CRACMM also predicts the lowest SOA concentrations across all scaling factors. AERO7 and SIMPLE are very similar in both response surface shape and magnitude. For each scheme, SOA concentrations decrease as the anthropogenic VOC emissions decrease. At TYL, the response surfaces for AERO7, Simple, and SOAP3 are similar, with SOA concentrations remaining relatively

575 constant at NO*x* scaling factors greater than 1. In contrast, CRACMM demonstrates a
576 much stronger response, with SOA mass increasing concurrently with NO*x* emissions.
577 At this biogenic-dominated site, SOA concentrations in all schemes are minimally
578 sensitive to variations in anthropogenic VOC emissions.
579 Understanding how SOA responds to NO*x* reductions is critical for near-term air
580 quality planning, as many regulatory strategies (e.g., cleaner vehicles, energy
581 transition) produce substantial NO*x* emissions abatement (Crippa et al. 2016; EPA et
582 al. 2017; Li et al. 2024). Table 4 summarizes the impact of a 50% reduction in NO*x*
583 emissions on total SOA, ASOA, and BSOA. In all schemes, reducing NO*x* leads to
584 increased ASOA concentrations, with the most pronounced increase predicted by
585 SOAP2. SIMPLE predicts the smallest increase in ASOA at DFW, while CRACMM
586 predicts the smallest increase at TYL. At DFW, this NO*x* reduction also drives an
587 increase in BSOA concentrations across most schemes, with the notable exception of
588 CRACMM. Consistent with the ASOA results, SOAP2 predicts the largest increase in
589 BSOA. The distinct behavior in CRACMM is driven by its monoterpene SOA
590 parameterization; contrary to other schemes and experimental evidence (Lane et al.
591 2008; Sarrafzadeh et al. 2016, Zhao et al. 2018), CRACMM predicts decreasing
592 yields under lower NO*x* conditions. Consequently, the substantial reduction in BSOA
593 predicted by CRACMM at DFW results in a net decrease in total SOA, a trend
594 opposite to that observed in the other schemes. At TYL, all schemes predict a
595 decrease in both BSOA and total SOA, with the most significant reductions observed
596 in the CRACMM simulation. The dominance of biogenic emissions at TYL compared
597 to DFW is reflected in the significantly higher BSOA concentrations. The differing
598 SOA responses to NO*x* reduction between the two sites are attributable to the distinct
599 biogenic emission regimes producing different VOC/NO*x* emission ratios.

Table 4 Average concentrations (μg/m^3) of anthropogenic SOA (ASOA) and biogenic SOA (BSOA) over days 2 through 5 for the base and reduced NOx model simulations. Shading indicates a decrease in SOA concentrations in the reduced NO*x* model runs compared to the base runs.

Location	Species	SOAP2			AERO7		
		Base	50% NO*x*	Diff (%)	Base	50% NO*x*	Diff (%)
DFW	ASOA	1.34	1.48	9.60%	2.34	2.38	1.90%
	BSOA	0.42	0.48	12.20%	0.41	0.42	0.40%
	Total SOA	1.76	1.96	10.30%	2.75	2.8	1.60%
TYL	ASOA	0.24	0.25	4.40%	0.28	0.31	9.90%
	BSOA	1.19	1.14	-4.10%	0.87	0.82	-6.20%
	Total SOA	1.43	1.4	-2.50%	1.16	1.14	-1.80%
Location	Species	CRACMM			Simple		
		Base	50% NO*x*	Diff (%)	Base	50% NO*x*	Diff (%)
DFW	ASOA	0.78	0.81	3.50%	2.44	2.45	0.60%
	BSOA	0.65	0.59	-10.70%	0.45	0.46	2.40%
	Total SOA	1.43	1.4	-2.50%	2.88	2.91	0.90%
TYL	ASOA	0.16	0.17	1.00%	0.3	0.32	8.50%
	BSOA	1.4	1.24	-12.60%	1.19	1.14	-4.40%
	Total SOA	1.56	1.41	-11.00%	1.49	1.46	-1.50%

4. Implications

SOA schemes implemented in CTMs are diverse, making quantitative comparisons inherently challenging. CTMs employ diverse approaches to simulate SOA, from simple schemes that treat SOApre as non-volatile to more complex VBS schemes that utilize multiple basis sets to represent different types of precursors. Variability in how SOA aging is treated further adds to the overall diversity across schemes. In our view, such diversity is valuable from a research perspective, given that the underlying processes driving SOA formation remain uncertain and, in many cases, poorly characterized. The variation in SOA yields across different schemes reflects the extent of these uncertainties. The differences in scheme formulation, coupled with the large numbers of parameters employed in some schemes, pose practical challenges for applying multiple schemes to standardized scenarios. Addressing these challenges may require innovative approaches. Nonetheless,

617 comparisons under standardized conditions are essential for achieving meaningful
618 quantitative inter-comparisons. Evaluating SOA yields under standard conditions and
619 plotting SOA yield curves (i.e., yield vs. C_{OA}) are effective strategies for identifying
620 similarities and differences among schemes. However, it is important to note that the
621 results presented here may not fully capture the ranges of conditions encountered in
622 three-dimensional atmospheric simulations.
623 **Non-aged SOA yields vary substantially across schemes and while many schemes**
624 **consider SOA aging, the aging effects vary.** Evaluating seven precursor types under
625 both high and low NO*x* conditions yields 14 distinct comparisons. Across these
626 comparisons, the ratio of maximum to minimum non-aged yields (max/min) ranges
627 from 1.8 to >1000 with a median max/min of 4.2 (Table 2). Among the eight schemes
628 examined, three (CAMx SOAP2, GEOS-Chem schemes) do not include explicit SOA
629 aging processes. Four schemes account for aging in a subset of precursor types and/or
630 NO*x*-conditions, while only one (CMAQ CRACMM) includes aging for all
631 precursors. Aging mechanisms considered by these schemes include gas-phase
632 OH-oxidation of evaporated SOA, particle-phase oligomerization, hydrolysis, and
633 photolysis. The impacts of aging on SOA yields vary by scheme and precursor (Table
634 S20): in 67 of the 98 evaluated cases (defined as one scheme/precursor/NO*x*-condition
635 combination, CRACMM excluded), aging has no effect; in 31 cases, it increases SOA
636 yields. Considering the aging effects, the ratio of max/min aged yields ranges from
637 5.0 to > 70, with a median value of 8.3 (Table 3). The relative rankings of precursors
638 by their initial/aged SOA yields differ across schemes (Table S21 and Table S22),
639 indicating that different aging schemes can lead to divergent conclusions regarding
640 the relative importance of specific SOA precursors—a consideration with potential
641 implications for policy guidance. For instance, discrepancies in yields lead to different
642 precursor rankings (e.g., the relative importance of aromatics vs. IVOCs). A model
643 that underpredicts the SOA potential of IVOC emissions might disproportionately

644 focus policy strategies on traditional VOCs (e.g., from petroleum-based solvents) and
645 potentially lead to ineffective widespread controls that miss the critical contribution of
646 IVOCs.
647 SOA aging remains an area in need of improved representation, with careful attention
648 required to ensure consistent underlying assumptions. Notably, only the two CAMx
649 schemes incorporate condensed-phase SOA photolysis, despite growing evidence that
650 both anthropogenic and biogenic SOA can undergo substantial photolytic depletion
651 (Hodzic et al., 2016; Baboomian et al., 2020), although a portion of SOA appears
652 recalcitrant to such degradation (O'Brien and Kroll, 2019).
653 **Large uncertainty exists for IVOC SOA yields.** The SOA yields from IVOCs show
654 wider variation (from negligible to 1.0 g/g) than for other anthropogenic precursors
655 (Table 2 and Table 3), partly due to different assumptions across schemes. For
656 example, schemes such as WRF-Chem MOSAIC and CHIMERE VBS predict very
657 low non-aged yields from IVOC, based on the assumption that several generations of
658 oxidation are required before forming condensable products. Even after one day of
659 aging, IVOC SOA yields remain highly variable, ranging from 0.02 to 1.20 g/g.
660 Although IVOC are generally classified based on volatility, factors such as high
661 molecular weight or the presence of polar functional groups can shift compounds into
662 the IVOC volatility range (Pankow and Asher, 2008). As a result, volatility and SOA
663 yield are not necessarily well correlated (Donahue et al., 2011). Improving model
664 representations of IVOC-derived SOA yields will require more detailed differentiation
665 of IVOC emissions into multiple subtypes, as illustrated by the CRACMM scheme
666 (Pye et al. 2023). A unified classification or "lumping" scheme for IVOC would be
667 particularly advantageous, allowing multiple models to utilize a common emissions
668 framework and enabling more direct comparisons of IVOC SOA yields. Improving
669 the representation of oxygenated VOCs with reduced volatility—such as glycols and
670 glycol ethers—within gas-phase chemical mechanisms can also support improved

differentiation of IVOC-related SOA formation (Yarwood and Tuite, 2024; Yu et al., 2024). More generally, a yield-based lumping approach for IVOCs (e.g., categorizing them into low, medium, or high yield classes) may be more practical to implement than strictly chemically-based schemes.

Determining experimental SOA yields also presents significant challenges. Laboratory experiments play a crucial role in guiding SOA model development and constraining key model parameters, particularly yields. However, these experiments are subject to operational and design limitations, including the need to account for chamber wall effects (Zhang et al., 2014) and to achieve atmospherically relevant concentration ranges (Peng et al., 2022; Kenagy et al., 2024). The role of autoxidation reactions in SOA formation further complicates the design of atmospherically relevant experiments, as discussed in detail by Kenagy et al. (2024). For instance, studying a reaction mechanism that includes RO_2 radical autoxidation at a rate of 0.1 s^{-1} requires that the effective rates of competing bimolecular reactions, particularly RO_2 + NO, be reduced to 0.1 s^{-1} or lower. This necessitates NO mixing ratios below approximately 5 ppb, which are now typical of photochemically active urban environments such as Los Angeles (Praske et al., 2018). Many SOA chamber experiments designed to investigate high NO*x* conditions exceed 5 ppb NO, thereby preventing autoxidation. Some chamber experiments, such as those by Sarrafzadeh et al. (2016), have been specifically designed to achieve atmospherically relevant NO (and other radicals) concentrations, making their results particularly valuable for SOA model development. In contrast, oxidation flow reactors face greater challenges (Peng et al., 2019) than chamber experiments in studying SOA formation due to their amplification of radical concentrations, which significantly shortens RO_2 lifetime and effectively suppresses autoxidation reactions. Wennberg (2023) has suggested shifting from the conventional terminology of high/low NO*x* to high/low NO to emphasize the critical role of NO concentration in determining RO_2 radical fate.

5. Conclusions

In this study, we compared SOA formation by eight schemes implemented in five widely used CTMs. For each SOA scheme, we quantified the non-aged SOA mass yields under standardized conditions (T=298 K and C_{OA}=10 μg/m^3), showed how the non-aged yield varies with C_{OA}, and quantified how one day of simulated atmospheric aging changed the non-aged yield. We calculated yields for 7 SOA precursor types (4 anthropogenic and 3 biogenic) under both high and low NO*x* conditions.

The lack of consistency across eight current SOA schemes reviewed here reveals a lack of consensus within the air quality modelling community, notwithstanding substantial efforts to greatly expand the scientific knowledge base related to SOA formation over recent decades. Evaluating SOA schemes using ambient measurements is unlikely to produce consensus because large uncertainties in the SOA schemes are confounded with large uncertainties in precursor emission estimates. In our view, there is no objective basis for preferring one SOA scheme over another considering the high degree of uncertainty presented here. Complex SOA schemes may be valuable to research for investigating linkages between precursors and SOA, but conversely, complexity may be a hindrance to the work of air quality planning because it adds to computational burdens and makes the science more difficult to comprehend and communicate. Notably, very simple SOA schemes have performed as well or better than complex schemes in their ability to simulate ambient OA measurements when driven by ambient precursor measurements (Hodzic and Jimenez, 2011; Pai et al., 2020). Complex schemes can introduce responses to conditions, such as NO*x* concentration, that may be unexpected and should be overtly evaluated if they have policy relevance, such as the NO*x* effect on SOA yield from BVOC. Simple schemes with well-characterized SOA yields and responses can have an important place in air quality modelling to support decision making which includes studies that value the health-burdens of air pollution as well as traditional emissions management

planning.

In addition, a majority of the eight schemes reviewed here are based on the VBS approach and we expect that sampling a larger number of model schemes would not change this finding. VBS schemes have practical advantages because experimental studies frequently summarize their data (e.g., SOA yields, POA volatility) in a VBS frame which makes for direct translation of these data into a VBS model scheme. However, VBS data can be translated into a different frame (e.g., a two-product scheme) for SOA formation or for representing the partial evaporation of POA emissions, as illustrated by Huang et al. (2024). Therefore, scheme developers can consider using non VBS-based approaches to gain advantages of simplicity and efficiency. The findings summarized above underscore the importance of understanding the limitations of available SOA schemes when applied to air quality management and policy development. The choice of model/scheme can significantly influence the predicted SOA concentrations and their evolution over time, which in turn affects air quality forecasts, assessments and regulations.

DATA AVAILABILITY

The source data for the figures, including an example of the offline calculation (i.e. CMAQ AERO7), are available at Zenodo (https://doi.org/10.5281/zenodo.16757660). Calculation data for other species and schemes are available from the corresponding authors upon request.

AUTHOR CONTRIBUTIONS

G.Y. and L.H. designed the research. L.H. performed the data collection, yields calculation, and data analysis. K.T. performed the box model calculation. L.H. K. T., and G.Y. wrote the manuscript. B. C., Z. W., K.T., P.V., and L.L. contributed to data analysis and revision of the manuscript. All authors contributed to the manuscript preparation and discussions.

ACKNOWLEDGMENTS

This work is supported by the Shanghai Technical Service Center of Science and Engineering Computing, Shanghai University. This study was financially supported

by the National Natural Science Foundation of China (Grant No. 42375103, 42375102) and Electric Power Research Institute (EPRI), Palo Alto, California.

COMPETING INTERESTS

The authors declare no competing interests.

REFERENCES

Appel, K. W., Bash, J. O., Fahey, K. M., Foley, K. M., Gilliam, R. C., Hogrefe, C., ... & Wong, D. C. (2021). The Community Multiscale Air Quality (CMAQ) model versions 5.3 and 5.3. 1: system updates and evaluation. *Geoscientific Model Development*, *14*(5), 2867-2897.

Baboomian, V.J., Gu, Y. and Nizkorodov, S.A., 2020. Photodegradation of secondary organic aerosols by long-term exposure to solar actinic radiation. *ACS Earth and Space Chemistry*, *4*(7), pp.1078-1089.

Cappa, C. D., & Wilson, K. R. (2012). Multi-generation gas-phase oxidation, equilibrium partitioning, and the formation and evolution of secondary organic aerosol. Atmospheric Chemistry and Physics, 12(20), 9505-9528.

Chang, X., Zhao, B., Zheng, H., Wang, S., Cai, S., Guo, F., ... & Donahue, N. M. (2022). Full-volatility emission framework corrects missing and underestimated secondary organic aerosol sources. *One Earth*, 5(4), 403-412.

Chen, Q., Miao, R., Geng, G., Shrivastava, M., Dao, X., Xu, B., ... & Zhu, T. (2024). Widespread 2013-2020 decreases and reduction challenges of organic aerosol in China. *Nature Communications*, 15(1), 4465.

Crippa, M., Janssens-Maenhout, G., Dentener, F., Guizzardi, D., Sindelarova, K., Muntean, M., et al. (2016). Forty years of improvements in Eu ropean air quality: Regional policy-industry interactions with global impacts. *Atmospheric Chemistry and Physics*, 16(6), 3825–3841.

CHIMERE Users Guide (2023). https://www.lmd.polytechnique.fr/chimere/, accessed on Feb. 15th 2024.

Couvidat, F., Bessagnet, B., Garcia-Vivanco, M., Real, E., Menut, L., & Colette, A. (2018). Development of an inorganic and organic aerosol model (CHIMERE 2017 β v1. 0): Seasonal and spatial evaluation over Europe. *Geoscientific Model Development*, *11*(1), 165-194.

Donahue, N. M., Robinson, A. L., Stanier, C. O., & Pandis, S. N. (2006). Coupled partitioning, dilution, and chemical aging of semivolatile organics. *Environmental science & technology*, *40*(8), 2635-2643.

Donahue, N. M., Epstein, S. A., Pandis, S. N., & Robinson, A. L. (2011). A two-dimensional volatility basis set: 1. organic-aerosol mixing thermodynamics. *Atmospheric Chemistry and Physics*, *11*(7), 3303-3318.

Emery, C.A., Baker, K.R., Wilson, G.M. and Yarwood, G. (2024). Comprehensive Air Quality Model With Extensions, v7. 20: Formulation and Evaluation for Ozone and Particulate Matter Over the US. *Geoscientific Model Development Discussions*, *2024*, pp.1-48.

EPA. (2017). United States environmental protection agency: Overview of the clean air Act and air pollution. https://www.epa.gov/clean-air-act-overview, accessed on March 5th, 2026

Hodzic, A. and Jimenez, J.L. (2011). Modeling anthropogenically controlled secondary organic aerosols in a megacity: A simplified framework for global and climate models. Geoscientific Model Development, 4(4), pp.901-917.

Hodzic, A., Jimenez, J. L., Madronich, S., Canagaratna, M. R., DeCarlo, P. F., Kleinman, L., & Fast, J. (2010). Modeling organic aerosols in a megacity: potential contribution of semi-volatile and intermediate volatility primary organic compounds to secondary organic aerosol formation. *Atmospheric Chemistry and Physics*, *10*(12), 5491-5514.

Hodzic, A.; Kasibhatla, P. S.; Jo, D. S.; Cappa, C. D.; Jimenez, J. L.; Madronich, S.; Park, R. J. Rethinking the global secondary organic aerosol (SOA) budget: stronger production, faster removal, shorter lifetime. Atmos. Chem. Phys. 2016, 16, 7917−7941.

Huang, L., Liu, H., Yarwood, G., Wilson, G., Tao, J., Han, Z., ... & Li, L. (2023). Modeling of secondary organic aerosols (SOA) based on two commonly used air quality models in China: Consistent S/IVOCs contribution but large differences in SOA aging. *Science of The Total Environment*, *903*, 166162.

Huang, L., Zi'ang Wu, H. L., Yarwood, G., Huang, D., Wilson, G., Chen, H., ... & Li, L. (2024). An improved framework for efficiently modeling organic aerosol (OA) considering primary OA evaporation and secondary OA formation from VOCs, IVOCs, and SVOCs.

Huang, R. J., Zhang, Y., Bozzetti, C., Ho, K. F., Cao, J. J., Han, Y., ... & Prévôt, A. S. (2014). High secondary aerosol contribution to particulate pollution during haze events in China. Nature, 514(7521), 218-222.

Koo, B., Knipping, E., & Yarwood, G. (2014). 1.5-Dimensional volatility basis set approach for modeling organic aerosol in CAMx and CMAQ. *Atmospheric Environment*, *95*, 158-164.

827 Lane, T. E., Donahue, N. M., & Pandis, S. N. (2008). Simulating secondary organic
828 aerosol formation using the volatility basis-set approach in a chemical
829 transport model. *Atmospheric Environment,* 42(32), 7439-7451.

830 Li, J., Zhang, H., Li, L., Ye, F., Wang, H., Guo, S., ... & Hu, J. (2023). Modeling
831 Secondary Organic Aerosols in China: State of the Art and Perspectives.
832 *Current Pollution Reports*, 9(1), 22-45.

833 Li, H., Zheng, B., Lei, Y., Hauglustaine, D., Chen, C., Lin, X., ... & He, K. (2024).
834 Trends and drivers of anthropogenic NOx emissions in China since
835 2020. *Environmental Science and Ecotechnology*, 21, 100425.

836 O'Brien, R.E. and Kroll, J.H. (2019). Photolytic aging of secondary organic aerosol:
837 Evidence for a substantial photo-recalcitrant fraction. *The journal of physical*
838 *chemistry letters*, *10*(14), pp.4003-4009.

839 Pankow, J.F. and Asher, W.E., 2008. SIMPOL. 1: a simple group contribution method
840 for predicting vapor pressures and enthalpies of vaporization of
841 multifunctional organic compounds. Atmospheric Chemistry and Physics,
842 8(10), pp.2773-2796.

843 Pai, S. J., Heald, C. L., Pierce, J. R., Farina, S. C., Marais, E. A., Jimenez, J. L., ... &
844 Vu, K. (2020). An evaluation of global organic aerosol schemes using airborne
845 observations. *Atmospheric Chemistry and Physics*, *20*(5), 2637-2665.

846 Pankow, J. F. (1994). An absorption model of the gas/aerosol partitioning involved in
847 the formation of secondary organic aerosol. *Atmospheric Environment*, *28*(2),
848 189-193.

849 Pennington, E. A., Seltzer, K. M., Murphy, B. N., Qin, M., Seinfeld, J. H., & Pye, H.
850 O. (2021). Modeling secondary organic aerosol formation from volatile
851 chemical products. *Atmospheric Chemistry and Physics*, 21(24), 18247-18261.

852 Pennington, Elyse A., Yuan Wang, Benjamin C. Schulze, Karl M. Seltzer, Jiani Yang,
853 Bin Zhao, Zhe Jiang et al. "An updated modeling framework to simulate Los
854 Angeles air quality–Part 1: Model development, evaluation, and source
855 apportionment." *Atmospheric Chemistry and Physics* 24, no. 4 (2024):
856 2345-2363.

857 Pye, H. O. T., Chan, A. W. H., Barkley, M. P., & Seinfeld, J. H. (2010). Global
858 modeling of organic aerosol: the importance of reactive nitrogen (NO*x* and
859 NO_3). *Atmospheric Chemistry and Physics*, *10*(22), 11261-11276.

860 Pye, H.O., Pinder, R.W., Piletic, I.R., Xie, Y., Capps, S.L., Lin, Y.H., Surratt, J.D.,
861 Zhang, Z., Gold, A., Luecken, D.J. and Hutzell, W.T. (2013). Epoxide
862 pathways improve model predictions of isoprene markers and reveal key role

of acidity in aerosol formation. Environmental Science & Technology, 47(19), pp.11056-11064.

Pye, Havala OT, Cavin K. Ward-Caviness, Ben N. Murphy, K. Wyat Appel, and Karl M. Seltzer. "Secondary organic aerosol association with cardiorespiratory disease mortality in the United States." *Nature Communications* 12, no. 1 (2021): 7215.

Pye, H. O., Place, B. K., Murphy, B. N., Seltzer, K. M., D'Ambro, E. L., Allen, C., ... & Stockwell, W. R. (2023). Linking gas, particulate, and toxic endpoints to air emissions in the Community Regional Atmospheric Chemistry Multiphase Mechanism (CRACMM). *Atmospheric Chemistry and Physics*, *23*(9), 5043-5099.

Ramboll (2022). CAMx User's Guide, Version 7.20. Retrieved from https://www.camx.com/download/source/, accessed on Feb. 15th, 2024

Robinson, A. L., Donahue, N. M., Shrivastava, M. K., Weitkamp, E. A., Sage, A. M., Grieshop, A. P., ... & Pandis, S. N. (2007). Rethinking organic aerosols: Semivolatile emissions and photochemical aging. *Science*, *315*(5816), 1259-1262.

Sarrafzadeh, M., Wildt, J., Pullinen, I., Springer, M., Kleist, E., Tillmann, R., Schmitt, S.H., Wu, C., Mentel, T.F., Zhao, D. and Hastie, D.R. (2016). Impact of NO x and OH on secondary organic aerosol formation from β-pinene photooxidation. *Atmospheric Chemistry and Physics*, *16*(17), pp.11237-11248.

Sasidharan, S., He, Y., Akherati, A., Li, Q., Li, W., Cocker, D., ... & Jathar, S. H. (2023). Secondary organic aerosol formation from volatile chemical product emissions: Model parameters and contributions to anthropogenic aerosol. *Environmental Science & Technology*, 57(32), 11891-11902.

Schell, B., Ackermann, I. J., Hass, H., Binkowski, F. S., & Ebel, A. (2001). Modeling the formation of secondary organic aerosol within a comprehensive air quality model system. *Journal of Geophysical Research: Atmospheres*, *106*(D22), 28275-28293.

Shrivastava, M., Easter, R. C., Liu, X., Zelenyuk, A., Singh, B., Zhang, K., ... & Tiitta, P. (2015). Global transformation and fate of SOA: Implications of low-volatility SOA and gas-phase fragmentation reactions. *Journal of Geophysical Research: Atmospheres*, *120*(9), 4169-4195.

Shrivastava, M., Fast, J., Easter, R., Gustafson Jr, W. I., Zaveri, R. A., Jimenez, J. L., ... & Hodzic, A. (2011). Modeling organic aerosols in a megacity: comparison of simple and complex representations of the volatility basis set approach. *Atmospheric Chemistry and Physics*, *11*(13), 6639-6662.

Strader, R., Lurmann, F., & Pandis, S. N. (1999). Evaluation of secondary organic aerosol formation in winter. *Atmospheric Environment*, *33*(29), 4849-4863.

Tsimpidi, A. P., Karydis, V. A., Pandis, S. N., & Lelieveld, J. (2016). Global combustion sources of organic aerosols: model comparison with 84 AMS factor-analysis data sets. *Atmospheric Chemistry and Physics*, 16(14), 8939-8962.

Vitali, Bruno, Manuel Bettineschi, Arineh Cholakian, Dino Zardi, Federico Bianchi, Victoria A. Sinclair, Johannes Mikkola et al. "Analysis of chemical and transport processes of biogenic aerosols over the northern Apennines: insights from the WRF-CHIMERE model." *Environmental Science: Atmospheres* 4, no. 9 (2024): 967-987.

Wildt, J., Mentel, T.F., Kiendler-Scharr, A., Hoffmann, T., Andres, S., Ehn, M., Kleist, E., Müsgen, P., Rohrer, F., Rudich, Y. and Springer, M. (2014). Suppression of new particle formation from monoterpene oxidation by NO*x*. *Atmospheric Chemistry and Physics*, *14*(6), pp.2789-2804.

WRF-Chem version 4.4 Users Guide. (2022). https://ruc.noaa.gov/wrf/wrf-chem/Users_guide.pdf, accessed on Feb. 15th 2024.

Yarwood, G. and Tuite, K., 2024. Representing Ozone Formation from Volatile Chemical Products (VCP) in Carbon Bond (CB) Chemical Mechanisms. Atmosphere, 15(2), p.178.

Yu, H., Møller, K.H., Buenconsejo, R.S., Crounse, J.D., Kjaergaard, H.G. and Wennberg, P.O., 2023. Atmospheric Photo-Oxidation of 2-Ethoxyethanol: Autoxidation Chemistry of Glycol Ethers. The Journal of Physical Chemistry A, 127(45), pp.9564-9579.

Zawadowicz, M. A., Lee, B. H., Shrivastava, M., Zelenyuk, A., Zaveri, R. A., Flynn, C., ... & Shilling, J. E. (2020). Photolysis controls atmospheric budgets of biogenic secondary organic aerosol. Environmental Science & Technology, 54(7), 3861-3870.

Zhang, Q. J., Beekmann, M., Drewnick, F., Freutel, F., Schneider, J., Crippa, M., ... & Perrussel, O. (2013). Formation of organic aerosol in the Paris region during the MEGAPOLI summer campaign: evaluation of the volatility-basis-set approach within the CHIMERE model. *Atmospheric Chemistry and Physics*, *13*(11), 5767-5790.

Zhang, X., Cappa, C. D., Jathar, S. H., McVay, R. C., Ensberg, J. J., Kleeman, M. J., & Seinfeld, J. H. (2014). Influence of vapor wall loss in laboratory chambers on yields of secondary organic aerosol. *Proceedings of the National Academy of Sciences*, 111(16), 5802-5807.

938 Zhao, D., Schmitt, S. H., Wang, M., Acir, I. H., Tillmann, R., Tan, Z., ... & Mentel, T.
939 F. (2018). Effects of NOx and SO2 on the secondary organic aerosol
940 formation from photooxidation of α-pinene and limonene. Atmospheric
941 Chemistry and Physics, 18(3), 1611-1628.

942 Zhao, Y., Hennigan, C. J., May, A. A., Tkacik, D. S., de Gouw, J. A., Gilman, J. B., ...
943 & Robinson, A. L. (2014). Intermediate-volatility organic compounds: a large
944 source of secondary organic aerosol. *Environmental Science &*
945 *Technology*, *48*(23), 13743-13750.

946 Zhao, B., Wang, S., Donahue, N. M., Jathar, S. H., Huang, X., Wu, W., ... &
947 Robinson, A. L. (2016). Quantifying the effect of organic aerosol aging and
948 intermediate-volatility emissions on regional-scale aerosol pollution in China.
949 *Scientific reports,* 6(1), 28815.